CPT-11. In tumor sections after injections of RET siRNA or CPT-11 alone, red, indicating apoptotic cells, was slightly observed, but not in saline or Cont siRNA (Fig. 7). On the other hand, combination treatment with RET siRNA plus CPT-11 strongly induced apoptotic cells. These data also indicated that combination therapy was effective for MTC.

Discussion

In this study, we demonstrated that the combination with RET siRNA and CPT-11 could induce the growth inhibition of TT cells and tumor xenografts. Recently, RET siRNA delivered by chitosan-coated poly(isobutylcyanoacrylate) nanoparticles led to tumor growth inhibition after intratumoral administration in mice transplanted with NIH3T3 cells transformed with the ret/PTC1 gene;[25] however, it has been reported that the ret/PTC-1 signaling pathway was different between thyroid and fibroblast cells;[26] therefore, this is the first report that RET siRNA transfected with NP inhibited tumor growth in mice bearing TT cells.

The combination therapy *in vivo* revealed greater than additive effects in cytotoxicity *in vitro*. CPT-11 is known as an effective inhibitor of angiogenesis for endothelial cells in tumor as well as cytotoxic drug.[27] The mechanism of increasing growth inhibition for TT tumor xenografts by RET siRNA and CPT-11 was not clear, although inhibition of receptor tyrosine kinase in tumor cells could sensitize cells to CPT-11.[28,29] Overexpression of Bcl-2 has been observed in MTC,[30,31] and is associated with the poor response of MTC to chemotherapy. The expression of dominant-negative RET in TT cells decreased the expression of Bcl-2 and could reduce cell viability,[21] and the antitumor effect by CPT-11 was enhanced by the combination with RET inhibitor, CEP-751, for TT tumor xenografts.[10] As another possibility, RET has been shown to activate nuclear factor κB (NFκB) *via* the phosphatidylinositol-3-kinase/Akt pathway.[1] Akt mediates multiple cellular responses, such as survival signaling by NFκB activation and BAD inactivation, and cell cycle progression; therefore, inhibition of RET expression might modulate cellular sensitivity through the survival signaling pathway.[32,33] From these findings, the combination of RET siRNA and CPT-11 will have great potential for gene therapy in MTC.

In conclusion, we demonstrated that combining RET siRNA with CPT-11 resulted in significant greater growth suppression of TT cells and tumor xenografts *via* increased apoptosis. As the thyroid gland is anatomically accessible, future treatment of primary MTC tumors by direct intratumoral injection of siRNA/NP complex expressing mutated genes is possible. Thus, the combination of RET siRNA and CPT-11 may serve as a novel tool for gene therapy.

Acknowledgments

We thank Ms. Manami Kubo for assistance with the experimental work. This study was supported in part by the Japan Health Sciences Foundation, by the Ministry of Education, Culture, Sports, Science and Technology of Japan, and by the Open Research Center Project.

References

1 Kodama Y, Asai N, Kawai K *et al.* The RET proto-oncogene: a molecular therapeutic target in thyroid cancer. *Cancer Sci* 2005; 96: 143–8.
2 Moley JF. Medullary thyroid carcinoma. *Curr Treat Options Oncol* 2000; 4: 339–47.
3 Hansford JR, Mulligan LM. Multiple endocrine neoplasia type 2 and RET: from neoplasia to neurogenesis. *J Med Genet* 2000; 37: 817–27.
4 Treanor JJ, Goodman L, de SF *et al.* Characterization of a multicomponent receptor for GDNF. *Nature* 1996; 382: 80–3.
5 Santoro M, Melillo RM, Carlomagno F, Vecchio G, Fusco A. Minireview: RET: normal and abnormal functions. *Endocrinology* 2004; 145: 5448–51.
6 Cohen MS, Moley JF. Surgical treatment of medullary thyroid carcinoma. *J Intern Med* 2003; 253: 616–26.
7 Gimm O. Thyroid cancer. *Cancer Lett* 2001; 163: 143–56.
8 Jones RL, Judson IR. The development and application of imatinib. *Expert Opin Drug Saf* 2005; 4: 183–91.
9 de Groot JW, Zonnenberg BA, van Ufford-Mannesse PQ *et al.* A phase II trial of imatinib therapy for metastatic medullary thyroid carcinoma. *J Clin Endocrinol Metab* 2007; 92: 3466–9.
10 Strock CJ, Park JI, Rosen DM *et al.* Activity of irinotecan and the tyrosine kinase inhibitor CEP-751 in medullary thyroid cancer. *J Clin Endocrinol Metab* 2006; 91: 79–84.
11 Drosten M, Frilling A, Stiewe T, Putzer BM. A new therapeutic approach in medullary thyroid cancer treatment: inhibition of oncogenic RET signaling by adenoviral vector-mediated expression of a dominant-negative RET mutant. *Surgery* 2002; 132: 991–7.
12 Drosten M, Stiewe T, Putzer BM. Antitumor capacity of a dominant-negative RET proto-oncogene mutant in a medullary thyroid carcinoma model. *Hum Gene Ther* 2003; 14: 971–82.
13 Parthasarathy R, Cote GJ, Gagel RF. Hammerhead ribozyme-mediated inactivation of mutant RET in medullary thyroid carcinoma. *Cancer Res* 1999; 59: 3911–4.
14 Messina M, Robinson BG. Technology insight: gene therapy and its potential role in the treatment of medullary thyroid carcinoma. *Nat Clin Pract Endocrinol Metab* 2007; 3: 290–301.
15 Pai SI, Lin YY, Macaes B, Meneshian A, Hung CF, Wu TC. Prospects of RNA interference therapy for cancer. *Gene Ther* 2006; 13: 464–77.
16 Marsh DJ, Theodosopoulos G, Martin-Schulte K *et al.* Genome-wide copy number imbalances identified in familial and sporadic medullary thyroid carcinoma. *J Clin Endocrinol Metab* 2003; 88: 1866–72.
17 Hattori Y, Yoshizawa T, Koga K, Maitani Y. NaCl induced high cationic hydroxyethylated cholesterol-based nanoparticle-mediated synthetic small interfering RNA transfer into prostate carcinoma PC-3 cells. *Biol Pharm Bull* 2008; 31: 2294–301.
18 Hattori Y, Fukushima M, Maitani Y. Non-viral delivery of the connexin 43 gene with histone deacetylase inhibitor to human nasopharyngeal tumor cells enhances gene expression and inhibits in vivo tumor growth. *Int J Oncol* 2007; 30: 1427–39.
19 Yoshizawa T, Hattori Y, Hakoshima M, Koga K, Maitani Y. Folate-linked lipid-based nanoparticles for synthetic siRNA delivery in KB tumor xenografts. *Eur J Pharm Biopharm* 2008; 70: 718–25.
20 Hattori Y, Koga K, Izumisawa T *et al.* The distribution of mRNA expression and protein after hydrodynamic injection of transgene in mice. *Biol Pharm Bull* 2009; 32: 755–9.
21 Drosten M, Hilken G, Bockmann M *et al.* Role of MEN2A-derived RET in maintenance and proliferation of medullary thyroid carcinoma. *J Natl Cancer Inst* 2004; 96: 1231–9.
22 Kaczirek K, Schindl M, Weinhausel A *et al.* Cytotoxic activity of camptothecin and paclitaxel in newly established continuous human medullary thyroid carcinoma cell lines. *J Clin Endocrinol Metab* 2004; 89: 2397–401.
23 Moley JF, Wells SA, Dilley WG, Tisell LE. Reoperation for recurrent or persistent medullary thyroid cancer. *Surgery* 1993; 114: 1090–5.
24 Tisell LE, Dilley WG, Wells SA Jr. Progression of postoperative residual medullary thyroid carcinoma as monitored by plasma calcitonin levels. *Surgery* 1996; 119: 34–9.
25 de Mil, Bertrand JR, Fusco A *et al.* siRNA nanoformulation against the ret/PTC1 junction oncogene is efficient in an in vivo model of papillary thyroid carcinoma. *Nucleic Acids Res* 2008; 36: e2.
26 Barone MV, Sepe L, Melillo RM *et al.* RET/PTC1 oncogene signaling in PC Cl 3 thyroid cells requires the small GTP-binding protein Rho. *Oncogene* 2001; 20: 6973–82.
27 Ji Y, Hayashi K, Amoh Y *et al.* The camptothecin derivative CPT-11 inhibits angiogenesis in a dual-color imageable orthotopic metastatic nude mouse model of human colon cancer. *Anticancer Res* 2007; 27: 713–8.
28 Koizumi F, Kanzawa F, Ueda Y *et al.* Synergistic interaction between the EGFR tyrosine kinase inhibitor gefitinib ('Iressa") and the DNA topoisomerase I inhibitor CPT-11 (irinotecan) in human colorectal cancer cells. *Int J Cancer* 2004; 108: 464–72.
29 Shao RG, Cao CX, Shimizu T, O'Connor PM, Kohn KW, Pommier Y. Abrogation of an S-phase checkpoint and potentiation of camptothecin cytotoxicity by 7-hydroxystaurosporine (UCN-01) in human cancer cell lines, possibly influenced by p53 function. *Cancer Res* 1997; 57: 4029–35.
30 Wang HG, Reed JC. Mechanisms of Bcl-2 protein function. *Histol Histopathol* 1998; 13: 521–30.

doi: 10.1111/j.1349-7006.2010.01484.x
© 2010 Japanese Cancer Association

31 Hinze R, Gimm O, Taubert H *et al.* Regulation of proliferation and apoptosis in sporadic and hereditary medullary thyroid carcinomas and their putative precursor lesions. *Virchows Arch* 2000; 437: 256–63.
32 Ludwig L, Kessler H, Wagner M *et al.* Nuclear factor-kappaB is constitutively active in C-cell carcinoma and required for RET-induced transformation. *Cancer Res* 2001; 61: 4526-35.
33 Segouffin-Cariou C, Billaud M. Transforming ability of MEN2A-RET requires activation of the phosphatidylinositol 3-kinase/AKT signaling pathway. *J Biol Chem* 2000; 275: 3568–76.

Supporting Information

Additional Supporting Information may be found in the online version of this article:

Fig. S1. *In situ* hybridization of a ^{35}S-labeled antisense or sense probe generated against RET mRNA. Microautoradiographs in bright fields of Fig. 5A were enlarged. Black grains indicate RET mRNA expression. Scale bar: 500 μm.

Fig. S2. *In situ* hybridization of a ^{35}S-labeled antisense or sense probe generated against RET mRNA. Microautoradiographs in bright fields of Fig. 5B were enlarged. Black grains indicate RET mRNA expression. Scale bar: 50 μm.

Please note: Wiley-Blackwell are not responsible for the content or functionality of any supporting materials supplied by the authors. Any queries (other than missing material) should be directed to the corresponding author for the article.

© 2010 Japanese Cancer Association

Pharmaceutical Research (© 2009)
DOI: 10.1007/s11095-009-0018-9

Research Paper

Accelerated Blood Clearance Was Not Induced for a Gadolinium-Containing PEG-poly(L-lysine)-Based Polymeric Micelle in Mice

Huili Ma,[1] Kouichi Shiraishi,[2] Takuya Minowa,[1] Kumi Kawano,[1] Masayuki Yokoyama,[2,3] Yoshiyuki Hattori,[1] and Yoshie Maitani[1,4]

Received July 6 2009; accepted November 24 2009

Purpose. Accelerated blood clearance (ABC) is induced by repeated injections of PEGylated liposomes. In this study, the ABC was investigated for a gadolinium-containing PEG-poly(L-lysine)-based polymeric micelle (Gd-micelle) and PEGylated liposome (Gd-liposome) in mice.

Materials and Methods. Effects of the first injection of Gd-micelle on the tissue distribution of the second dose of Gd-micelle were studied. Additionally, effects of the first injection of Gd-micelle, Gd-liposome, empty liposome, polyethyleneglycol ($PEG_{500,000}$), and PEG-lipid on the distribution of the second dose of the Gd-liposome were evaluated.

Results. Results indicated that the tissue distribution of the second injection of the Gd-micelle at a dose of 33, 5, or 2 μmol Gd/kg was not affected by the first injection of the Gd-micelle at different doses and time intervals or of the empty PEGylated liposome 7 days before. ABC of Gd-liposome at a dose of 2.3 μmol Gd/kg (corresponding to 10 μmol lipids/kg) was observed when the empty PEGylated liposome or Gd-liposome, but not the Gd-micelle, $PEG_{500,000}$ or PEG-lipid, was pre-administered.

Conclusions. The hydrophobic core of the micelle or lipid bilayer of PEGylated liposome has a major effect on this phenomenon. These studies have significant implications for the evaluation of PEG-poly (L-lysine)-based micellar formulation of Gd-based contrast agents.

KEY WORDS: accelerated blood clearance; gadolinium; PEGylated liposome; polyethylene glycol (PEG); polymeric micelle.

INTRODUCTION

Long-circulating liposomes with surface-modified polyethyleneglycol (PEG) are often used as carriers of therapeutic agents, since they avoid capture by the reticuloendothelial system (RES) and can extend the systemic circulation time of agents, thereby improving drug delivery (1,2). It was hypothesized that PEG on the surface of liposomes forms a water shell, resulting in decreased adsorption of opsonins and subsequent phagocytosis by cells of the RES (3,4). However, PEGylated liposomes are known to lose their long-circulating property with multiple dosing. Recently, it has been reported that the first dose of PEGylated liposomes injected intravenously caused a loss of the long-circulating property and extensive accumulation in the liver at the second dose injected several days later in mice, rats, rabbit, and rhesus monkeys (5–11), a phenomenon known as accelerated blood clearance (ABC). Besides PEGylated liposomes, other nanocarriers, such as nanoparticles containing PEG, also produced this phenomenon (12). Therefore, ABC would have a significant impact on the application of long-circulating liposomes and nanoparticles with multiple administrations. In clinical applications of liposomal carriers, Gabizon *et al.* reported a reduced clearance of doxorubicin-containing PEGylated liposome in the repeated injections. This opposite behavior to the ABC phenomenon resulted from toxic activity of the encapsulated doxorubicin against the RES (13). Presently, the ABC phenomenon is not a problem in a cancer chemotherapy by the use of a PEG-liposomal carrier, whereas the ABC phenomenon in human clinics must be important for less toxic drug or gene delivery applications of the PEGylated liposomes.

To date, studies of ABC have focused mainly on PEGylated liposomes. Many factors can affect the extent to which ABC is induced by PEGylated liposomes. First of all, the dose of lipid plays an important role, with ABC enhanced at lower concentrations of lipid (6,7,12). Second, ABC occurs in a time-dependent manner (5,7). The time interval between the first and second doses is a key factor. Third, when the amount of PEGylated lipid in the first injection was ≤5 mol%, the second dose of PEGylated liposomes was eliminated more quickly from plasma than liposomes containing >10 mol% PEGylated lipid injected as a first dose (7,8). In addition, the ABC phenomenon

[1] Institute of Medicinal Chemistry, Hoshi University, 2-4-41 Ebara, Shinagawa-ku, Tokyo 142-8501, Japan.
[2] Kanagawa Academy of Science and Technology, Yokoyama "Nanomedical Polymer" Project, KSP East 408, Sakado 3-2-1, Takatsu-ku, Kawasaki, Kanagawa 213-0012, Japan.
[3] Medical Engineering Laboratory, Research Center for Medical Science, Jikei University School of Medicine, 3-25-8, Nishi-shinbashi, Minato-ku, Tokyo 105-8461, Japan.
[4] To whom correspondence should be addressed. (e-mail: yoshie@hoshi.ac.jp)

Published online: 25 December 2009

0724-8741/09/0000-0001/0 © 2009 Springer Science+Business Media, LLC

was reported to be independent of liposomal size, surface charge, and PEG molecular weight (*5,7,8*).

During the past decade, polymeric micelles, supramolecular assemblies of block copolymers, have demonstrated their utility in drug delivery systems and are currently recognized as promising nanocarriers for enhancing the efficacy of drugs and genes (14–16). Since ABC has a considerable impact on the multiple drug administration, it is necessary to study whether the phenomenon is induced by repeated injections of polymeric micelles. Gadolinium (Gd)-based contrast agents are widely used in magnetic resonance imaging (MRI) to improve the conspicuity of lesions or visualization of blood vessels (17). However, these agents are rapidly cleared from the circulation. To overcome this problem, nanocarriers, such as liposomes and polymeric micelles, are used to encapsulate the agents so as to prolong their circulation and allow them to accumulate in tumors for diagnosis (18–20). If polymeric micelles containing a diagnostic agent cause the ABC phenomenon, then circulation time will be reduced after a second dose and the accuracy of the diagnosis will be affected. Furthermore, polymeric micelles containing MRI agents or drugs administered during diagnosis and treatment will lose some of their drug efficacy because of the accelerated clearance. Hence, it is of great importance to know whether the ABC phenomenon can be induced by polymeric micelles or not. Recently, the accelerated clearance of [^{3}H]-labeled PEGylated liposomes was observed in mice pre-administered with an empty polymeric micelle composed of poly (ethylene glycol)-*b*-poly (β-benzyl L-aspartate) (PEG-PBLA) 50 nm in diameter (16).

In this study, we first investigated whether the ABC effect was caused by repeated injections of a polymeric micelle encapsulating Gd-DOTA (Gd-micelle) and of a PEGylated liposome encapsulating Gd-DTPA (Gd-liposome) as a positive control. Concentrations of Gd ions were measured for this investigation. Furthermore, we examined the effect of a PEG homopolymer on the tissue distribution of Gd-liposomes.

MATERIALS AND METHODS

Materials

Magnevist® (Gd-DTPA) was purchased from Bayer Schering Pharma (Berlin, Germany). 1,2-distearoyl-sn-glycero-3-phosphoethanolamine-n-[methoxy(polyethylene glycol)-2000] (mPEG$_{2000}$-DSPE), hydrogenated soy bean phosphatidylcholine (HSPC), and egg phosphatidylcholine (EPC) were purchased from the NOF Corporation (Tokyo, Japan). Cholesterol and polyethylene glycol 500,000 (PEG$_{500,000}$) were of analytical grade (Wako Pure Chemical, Osaka, Japan). All lipids were used without further purification. All other reagents were of analytical grade.

Animals

Four-week-old female ddY mice were purchased from Sankyo Lab Service Corp. (Tokyo, Japan). All care and handling of animals were performed with the approval of the Animal and Ethics Review Committee of Hoshi University and of Principles of Laboratory Animal Care (NIH #publication 85-23, revised in 1985).

Preparation of the Gd-micelle

Synthesis of a chelate moiety-binding block copolymer was performed as reported in our previous paper (19). Briefly, a poly(ethylene glycol)-*b*-poly(L-lysine) block copolymer (PEG-P(Lys)) was prepared through acid hydrolysis of a poly(ethylene glycol)-*b*-poly[ε-(benzyloxycarbonyl)-L-lysine] (PEG-P(Lys(Z)) block copolymer (Fig. 1). We synthesized PEG-P(Lys(Z) with polymerization of a Lys(Z) *N*-carboxy anhydride monomer from PEG-NH_2 (molecular weight of PEG-NH_2 = 5,200). 1,4,7,10-Tetraazacyclododecane-1,4,7,10-tetraacetic acid mono (*N*-hydroxysuccinimide ester) was fully conjugated to lysine residues of PEG-P(Lys).

The composition of PEG-P(Lys-DOTA) was determined by means of ^{1}H-NMR spectroscopy in D_2O under alkali conditions (pH>10). $GdCl_3{\cdot}6H_2O$ was added to PEG-P(Lys-DOTA) at pH 6.0 to 6.5 for 3 hr at 50°C. Gd content was determined using inductively coupled plasma (ICP) (SPS7800, SII Nano Technology Inc., Tokyo, Japan). We obtained the block copolymer as PEG-P(Lys-DOTA-Gd) (Gd content = 7.7 wt%, the number average of Gd is 8.2). The block copolymer formed a polymeric micelle spontaneously in an aqueous solution (Gd-micelle). The size and zeta-potential of the Gd-micelle diluted with saline for three independent preparations was 84.5±6.0 nm and −1.70±0.80 mV, respectively, at 25°C as determined by dynamic light scattering (ELS-Z2, Otsuka Electronics Co., Ltd., Osaka, Japan).

Preparation of the Empty Liposome and Gd-liposome

First, an empty liposome, which induced the ABC phenomenon, was prepared by the lipid film hydration method as described previously (21). Briefly, a mixture of HSPC, cholesterol, and mPEG$_{2000}$-DSPE in a molar ratio of 1.85:1.0:0.15 was dissolved in chloroform. The solution was

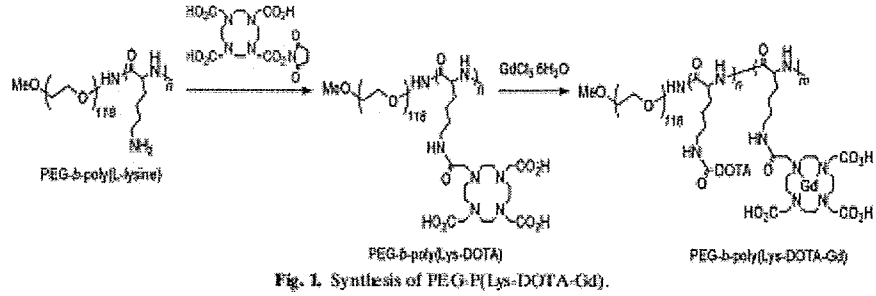

Fig. 1. Synthesis of PEG-P(Lys-DOTA-Gd).

evaporated dry to form the lipid film. Then, the liposome was produced by hydration of the lipid film with saline, followed by size reduction with sonication. The size and zeta-potential of the liposome diluted with saline were 178.5 nm and −22.1 mV, respectively.

Two kinds of Gd-liposomes were prepared because Gd-DTPA content was dependent on the preparation methods. One kind of Gd-liposome was prepared by an ethanol injection method (GdL-E). In brief, a mixture of EPC, cholesterol, and $mPEG_{2000}$-DSPE in a molar ratio of 2.15:0.85:0.15 was dissolved in ethanol and then hydrated with Gd-DTPA at 50°C. The resulting liposomes were sonicated for 10 min, then subjected to exhaustive dialysis against phosphate-buffered saline (PBS, 137 mM NaCl, 8.10 mM Na_2HPO_4, 2.68 mM KCl, 1.47 mM KH_2PO_4, pH 7.4) with a dialysis membrane having a 2,000 molecular-weight cutoff for 24 hr. The size and zeta-potential of the liposome were 150.1±18.8 nm and −0.94±6.78 mV, respectively, for three independent preparations. As a control of GdL-E, an empty liposome not including Gd-DTPA (empty GdL-E) was prepared by the same method as the Gd-liposome (GdL-E), except that saline was used to hydrate the ethanol solution of lipid. The particle size of empty GdL-E was 139.5 nm. Another kind of Gd-liposome was prepared by reverse phase evaporation (GdL-R) to encapsulate a larger amount of Gd-DTPA. The lipid was the same as GdL-E described above and dissolved in 4 mL of chloroform and 2 mL of diethyl ether. Gd-DTPA was added to the lipid solution. The mixture was sonicated to form an emulsion, which was evaporated to produce the liposome. Finally, the resulting liposome was sized at 60°C on an extruder (Avanti Polar Lipids, Inc., AL, USA) with three passes through a 0.4 μm Nuclepore membrane (Waterman, Maidstone, UK) and five passes through a 0.2 μm Nuclepore membrane, followed by exhaustive dialysis as described above. The particle size and zeta-potential of the liposome were 140.9± 13.5 nm and −2.52±5.18 mV, respectively, for three independent preparations. The phospholipid concentration of the liposome including HSPC or EPC was measured with the Phospholipids C-test Wako (Wako Pure Chemical Industries, Ltd.). GdL-E contained 2.26 μmol Gd per 10 μmol lipids, and GdL-R contained 2.29 μmol Gd per 5 μmol lipids.

Release Studies of Gd-micelle and Gd-liposomes

The release of Gd−DTPA from Gd−liposome (GdL−E or GdL−R) and Gd from Gd−micelle was evaluated by dialysis method using a Spectrapor 6 tubing with molecular weight cut-off of 1,000 Da (Spectrum Laboratories Inc., Tokyo, Japan). Briefly, the sample of Gd-micelle containing 1.2 mM Gd and Gd-liposomes of GdL-E containing 0.96 mM Gd-DTPA or GdL-R containing 0.96 mM Gd-DTPA (1 mL) were dialyzed against PBS (pH 7.4, 200 mL) at 37°C. At the indicated time points (10 min, 1, 3, 6, 24 h), 1 mL aliquots of the medium were withdrawn, and the same volume of fresh medium was added. The Gd concentration was analyzed by ICP. The accumulative release of Gd or Gd-DTPA released from the Gd-micelle or Gd-liposome, respectively was expressed as a percentage of the released Gd or Gd-DTPA and plotted as a function of time.

Pharmacokinetics and Tissue Distribution of the Gd-micelle and Gd-liposome

For pharmacokinetics study, the mice were intravenously injected with the Gd-micelle at a dose of 33 μmol Gd/kg (67.3 mg polymer/kg) or the Gd-liposomes including GdL-E at a dose of 6.75 μmol Gd/kg and 10 μmol lipids/kg and GdL-R at 2.65 μmol Gd/kg and 5 μmol lipids/kg. About 30 to 100 μL of blood were taken from a tail vein with a quantitative capillary at 10 min, 1 h, 3 h, 6 h, and 24 h after the injection. The Gd-micelle or the Gd-liposome was injected into a lower part of a tail vein, and blood sample was taken at a certain time point described above from an upper part of the tail vein at the other side of the injected vein. Therefore, this experiment was free from the sample pollution problem. The blood samples were added to saline and centrifuged at 3,000 rpm for 15 min, and the supernatant was used to measure Gd content by ICP. The elimination half-life ($T_{1/2}$) was calculated based on a single compartment model. For the tissue distribution of Gd-micelles and Gd-liposomes study, the second dose of Gd-micelles or Gd-liposomes was injected intravenously through the tail vein at a certain time interval after the first injection. Samples of blood were taken from the hepatic portal vein 6 h after the second injection, and tissues of liver, spleen, and kidney were removed at the same time. The plasma and blood volume were calculated as 0.0488 mL/g body weight for plasma and 0.0778 mL/g body weight for blood, respectively (19).

Measurement of Gd Content

For the quantitative determination of Gd content, blood samples were centrifuged at 3,000 rpm for 15 min, and then plasma was taken out and diluted with 0.1% HNO_3 for ICP. Tissue samples of the liver, spleen, and kidney were digested with a mixture of 98% H_2SO_4 and 62% HNO_3 (1:2, v:v) and then subjected to ICP.

Statistical Analysis

The statistical analysis was performed with the Dunnett's multiple comparison test. The level of significance was set at $p<0.05$ or $p<0.01$.

RESULTS

Release Behavior of Gd-micelle and Gd-liposomes

Gd or Gd-DTPA release behavior from Gd-micelle or Gd-liposomes was studied by the dialysis method. As shown in Fig. 2, only 0.2% of Gd leaked from the Gd-micelle at 37°C in PBS (pH 7.4) for 24 h. On the other hand, 4.8% of entrapped Gd-DTPA leaked from the Gd-liposome prepared by reverse phase evaporation method (GdL-R) and 22.4% for 24 h from the Gd-liposome prepared by ethanol injection method (GdL-E). Hence, it is obvious that Gd-micelle has hardly release behavior of Gd, and GdL-R showed much slower release than GdL-E. The results indicated that the leakage of Gd or Gd-DTPA from nanocarriers was greatly affected by the preparation methods.

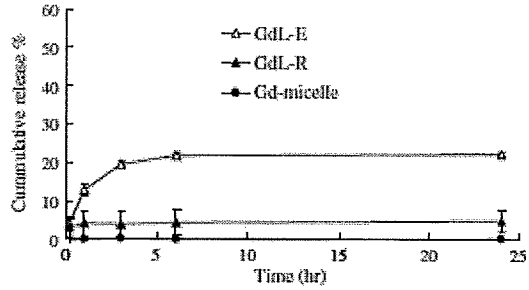

Fig. 2. Release profiles of Gd from Gd-micelle or Gd-DTPA from Gd-liposomes prepared by ethanol injection method (GdL-E) and reverse phase evaporation method (GdL-R) in PBS (pH 7.4) at 37°C. Data represent mean±S.D. (n=3).

Pharmacokinetics of the Gd-micelle and Gd-liposome

As shown in Fig. 3, at 10 min after the intravenous injection, 33.3% of the injected dose was found in blood for the Gd-micelle, and 40.0% and 50.3% for the Gd-liposome of GdL-E and GdL-R, respectively. At a dose of 33 μmol Gd/kg, the $T_{1/2}$ of the Gd-micelle was 10.2±3.9 h. Besides, the $T_{1/2}$ of GdL-E at a dose of 6.75 μmol Gd/kg and GdL-R at a dose of 2.65 μmol Gd/kg were 5.9±0.5 h and 6.0±1.0 h, respectively. In a previous study, we showed that Gd-DTPA was very rapidly cleared from the bloodstream with a minute's order half-life (19). Therefore, the detected Gd in blood is considered to be Gd-DTPA encapsulated in the liposome in a quantitative manner for measurements 6 h post intravenous injection. On the other hand, the main purpose of this study is the ABC phenomenon of a polymeric micelle MRI contrast agent, and PEGylated liposome is used as a positive control for the ABC phenomenon. Therefore, detection of liposome with Gd measurements is appropriate for the present purpose.

Effect of the First Dose on the Distribution of the Gd-micelle

The effects of the first dose on the distribution of the Gd-micelle injected a second time were evaluated. When the second dose of Gd-micelle was fixed at 33 μmol/kg, there was no significant difference of percent injected doses in plasma, kidney, and spleen between various first doses of the Gd-micelle from 0 to 100 μmol/kg (Fig. 4A). A dose of 100 μmol Gd/kg is the clinical dose of Gd-DTPA (17). Interestingly, the distribution of Gd-micelles in plasma, kidney, spleen and liver with the first injection of the empty liposome was similar to that with the first injection of saline. For the liver, the percent injected dose after a first dose of 33 μmol/kg and 100 μmol/kg was significantly higher than in the control saline group, possibly due to the incomplete elimination of the first dose of the Gd-micelle in liver at day 7 because of high doses of polymeric micelles (67.3 mg ~ 203.9 mg polymer/kg). The dose of 2 μmol Gd/kg of the Gd-micelle was the minimum at which Gd was detectable by means of ICP 6 h after injection. As shown in Fig. 4B, when the second dose of the Gd-micelle was decreased to 5 μmol/kg and 2 μmol/kg, the distribution was similar to that of 33 μmol/kg (Fig. 4A). Hence, the results showed that the tissue distribution of the Gd-micelle at the second dose of 33, 5, or 2 μmol/kg was not affected significantly except in liver by pre-administration of the Gd-micelle or the empty liposome. Although Gd in the first dose may interfere with the Gd accumulation in liver following the second dose injection, Gd-micelle as the first dose for micelle-forming properties are

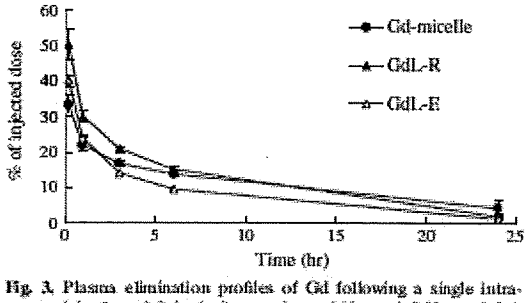

Fig. 3. Plasma elimination profiles of Gd following a single intravenous injection of Gd-micelle at a dose of 33 μmol Gd/kg and Gd-liposome including Gd-liposome prepared by ethanol injection method (GdL-E) at a dose of 6.75 μmol Gd/kg and Gd-liposome prepared by reverse phase evaporation method (GdL-R) at a dose of 2.65 μmol Gd/kg. Data represent mean±S.D. (n=3-4).

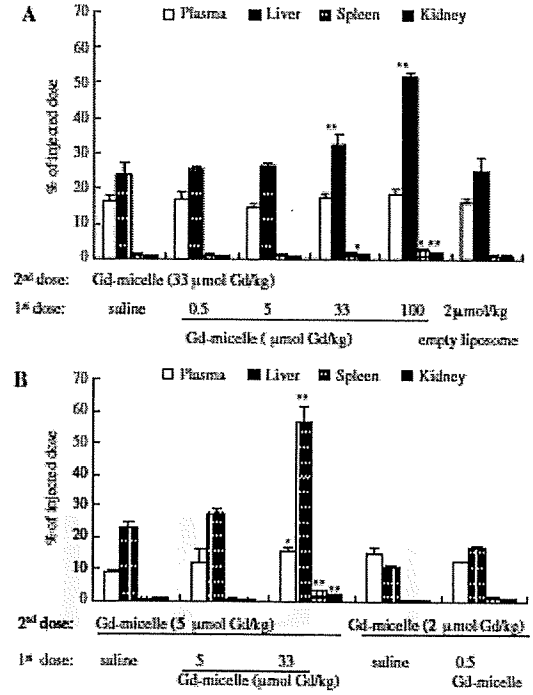

Fig. 4. Effect of the first dose on the tissue distribution of Gd-micelle. The second dose of Gd-micelle with 33 μmol/kg (**A**) or 5 μmol/kg or 2 μmol/kg (**B**) was intravenously injected at day 7 after the first injection of 0.5, 5, 33, 100 μmol/kg of Gd-micelle or the empty liposome at a dose of 2 μmol lipid/kg. Tissues including blood, liver, spleen, and kidney were taken out 6 h after the second injection of Gd-micelle. Data represent mean±S.D. (n=3, 6). P values apply to differences between the saline group and Gd-micelle or liposome treated group. $^{*}p<0.05$, $^{**}p<0.01$.

Gd-content-dependent, and Gd-free polymeric micelle is different from the Gd-containing micelle in size and micelle forming characteristics.

Effect of Time Interval Between the Two Injections on the Distribution of the Gd-micelle

Since it was reported that the ABC effect was maximized when the interval between the two injections of liposome was 10 days in mice (7,12), we changed the time interval for the injection of Gd-micelle at a dose of 33 μmol/kg from 3 days to 10 days. No significant difference in plasma Gd levels (15 ~ 18% dose) was observed between the control group and the groups with different time intervals 6 h after the second injection (Fig. 5). The control group was given the Gd-micelle at 33 μmol/kg after a first injection of saline. The Gd% of injected dose in the liver was much higher at day 3 after the second injection than that on other days, probably due to the incomplete elimination of the first dose of the Gd-micelle.

Effect of the First Dose on the Distribution of the Gd-liposome

Since a lower dose of lipid in the first injection results in a more significant ABC, the effects of dose were investigated. The first dose of the Gd-micelle (5 μmol Gd/kg), empty GdL-E (2 μmol lipids/kg), or GdL-E (2 μmol lipids/kg corresponding to 0.45 μmol Gd/kg) was given with a second dose of GdL-E at 10 μmol lipids/kg corresponding to 2.26 μmol Gd/kg. As shown in Fig. 6, the first injection of the Gd-micelle resulted in a similar percentage of the injected dose of the Gd-liposome in plasma, liver, spleen, and kidney in comparison with the saline group. On the other hand, after the second injection of GdL-E, the Gd concentrations in plasma and kidney were too low to be detected, with the first injection of the empty GdL-E and the GdL-E. At that time, the %dose in the liver significantly increased, but that in spleen significantly decreased as compared to saline ($p<0.05$).

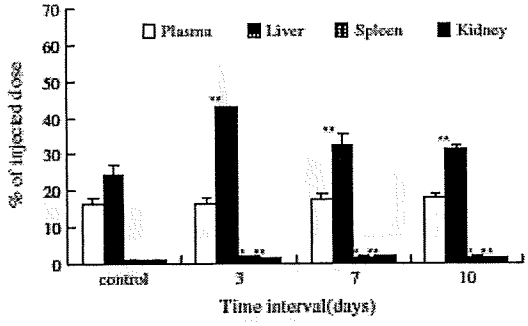

Fig. 5. Effect of the time intervals on the tissue distribution of Gd-micelle. The second dose of Gd-micelle at 33 μmol/kg was intravenously injected at day 3, day 7, or day 10 after the first injection of the same micelle at 33 μmol/kg. The control group was referred to the second dose of Gd-micelle at a dose of 33 μmol/kg with the first injection of saline. Tissues including blood, liver, spleen, and kidney were taken out at 6 h after the second injection of Gd-micelle. Data represent mean±S.D. ($n=3$). *P* values apply to differences between the control group and treated group. $^{*}p<0.05$, $^{**}p<0.01$.

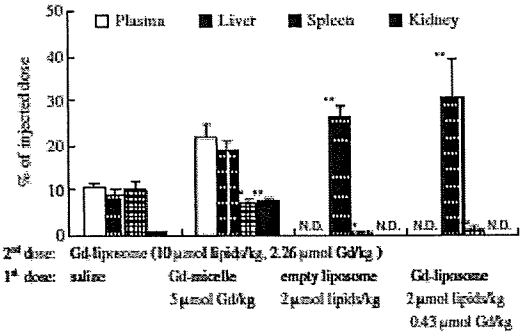

Fig. 6. Effect of the first dose on the tissue distribution of Gd-liposome (GdL-E). The second dose of GdL-E with 10 μmol lipids/kg and 2.26 μmol Gd/kg was intravenously injected at day 7 after the first injection of Gd-micelle (5 μmol Gd/kg), empty GdL-E (2 μmol lipids/kg), and GdL-E (2 μmol lipids/kg and 0.43 μmol Gd/kg). Tissues of blood, liver, spleen, and kidney were removed 6 h after the second injection of GdL-E liposome. Data represent mean±S.D. ($n=3$). *P* values apply to differences between the saline group and Gd-micelle or liposome treated group. $^{*}p<0.05$, $^{**}p<0.01$. N.D. The Gd concentration was too low to be detected by ICP.

Therefore, the data herein show that the accelerated clearance of Gd-liposome at 10 μmol lipids/kg corresponding to 2.26 μmol Gd/kg was induced by both the Gd-liposome and empty liposome, but not by the Gd-micelle. This finding indicates that Gd ions at the first dose of 0.45 μmol/kg did not affect the induction of ABC caused by liposomes.

Effect of PEG on the Distribution of Gd-liposomes

Next, the effect of injecting a PEG homopolymer and PEG_{2000}-DSPE on the distribution of Gd-liposomes was examined. Since the encapsulation efficiency of Gd was low with the ethanol injection method, we prepared another Gd-liposome by the reverse phase evaporation method (GdL-R). The tissue distribution of GdL-R at 6 h after injection at a dose of 5 μmol lipids/kg was not significantly influenced by the pre-administration of 50 mg/kg PEG $_{500,000}$ 0.2 mg/kg PEG $_{500,000}$, or 0.3 mg/kg PEG_{2000}-DSPE 7 days before (Fig. 7). The dose of 0.2 mg/kg PEG $_{500,000}$ and 0.3 mg/kg PEG_{2000}-DSPE with the concentration of 0.04 mg/ml is similar to that of the 5 mol% PEGylated liposome (0.3 mg/kg PEG_{2000}-DSPE), which could produce the ABC phenomenon (Fig. 6). Hence, the first injection of $PEG_{500,000}$ saline or PEG_{2000}-DSPE saline failed to cause the ABC phenomenon after the second administration of Gd-liposome. Hence, only injections of PEG macromolecules did not induce the ABC effect.

DISCUSSION

In the present study, the influence of dose on the tissue distribution of Gd-micelles after repeated administrations was investigated. Many studies have found that a lower dose of lipid in liposomes or nanoparticles results in a greater ABC effect (6–8,12), and the magnitude of the ABC phenomenon reached a maximum when the time interval between two

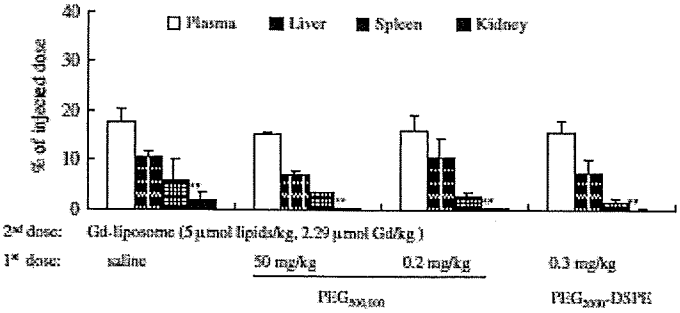

Fig. 7. Effect of $PEG_{500,000}$ and PEG_{2000}-DSPE on the tissue distribution of Gd-liposome (GdL-R). The second dose of Gd-liposome with 5 μmol lipids/kg and 2.29 μmol Gd/kg was intravenously injected at day 7 after the first injection of $PEG_{500,000}$ saline at a dose of 50 mg/kg or 0.2 mg/kg, and PEG_{2000}-DSPE saline at 0.3 mg/kg. The control group of GdL-R was injected at a dose of 10 μmol lipids/kg with the first injection of saline. Tissues of blood, liver, spleen, and kidney were removed at 6 h after the second injection of GdL-R. Data represent mean±S.D. (n=3–5). P values apply to differences between the saline group and $PEG_{500,000}$ or PEG_{2000}-DSPE treated group. $^{*}p<0.05$, $^{**}p<0.01$.

injections was 5–7 days in rats (5) and 10 days in mice (7,12). Hence, we investigated the distribution of the Gd-micelle at various doses and an interval of 3, 7, or 10 days between injections. We found that repeated injections of the Gd-micelle, even with the second dose reduced to 2 μmol Gd/kg (corresponding to 4 mg polymer/kg) and at different time intervals at a dose of 33 μmol Gd/kg (corresponding to 67.3 mg polymer/kg), did not result in an accelerated clearance. ABC of the second injection of the Gd-liposome was induced by the first injection of both the Gd-liposome and the empty PEGylated liposome, but not by the first injection of the Gd-micelle (Fig. 6), Gd-DTPA encapsulated in liposomes would not affect the ABC phenomenon. Therefore, our observation that the ABC phenomenon did not occur with the Gd-micelle is important as it means that injections of the Gd-micelle will not change the biodistribution of a second administration of diagnostic or therapeutic agents.

For Gd-micelle, Gd was chelated to the micelle and thus existed in the form of micelle as shown in Fig. 1, which was consistent with the release results in Fig. 2 that Gd did not leak from the Gd-micelle in PBS (pH 7.4). Gd concentration in plasma, therefore, will reflect the pharmacokinetic behavior of the Gd-micelle. For Gd-liposomes, although the Gd concentration in plasma contained both the leaked Gd-DTPA from the Gd-liposome and the encapsulated Gd-DTPA in the Gd-liposome, the leaked-free Gd-DTPA is reported to be very rapidly cleared from the bloodstream with a minute's order half-life (19), and thus the detected Gd in blood is considered to be only the Gd-DTPA encapsulated in the liposome 6 h after intravenous injection in this study. Compared to GdL-R, the leakage of Gd-DTPA from GdL-E was faster, resulting in the lower Gd concentration (the encapsulated Gd) of GdL-E in blood in Fig. 3. Most importantly, the purpose of this study is to investigate if the distribution for the second dose of the Gd-liposomes or Gd-micelle was affected after pre-administered with the first dose or not. Therefore, the leakage of Gd-DTPA from the Gd-liposomes will not influence this study. In addition, many studies demonstrated that ABC phenomenon for empty liposome was observed determined by [^{3}H]-labelled or ^{99m}Tc-labelled method (5–9).

It is believed that macrophages in the RES play an important role in ABC, and liposomes were mainly located in Kupffer cells after a second injection (5,8). When hepatosplenic macrophages were depleted, no enhanced clearance of liposomes was observed (6). The induction of ABC with liposomes could be attributable to a 150 kDa serum factor (5), anti-PEG IgM (9,11,12,22,23), anti-PEG antibody (10), or anti-PEG IgG antibody (24).

Whereas the mechanism of the immune response on repeated injections of liposomes has not been fully elucidated yet, the enhanced clearance effect can still be divided into two phases: the induction phase following the first injection and the effectuation phase following the second injection (6). According to this theory, there are two very important factors: one is the biological material (e.g. antibody) produced in the induction phase, the other is the recognition of the antibody by the second dose. For the effectuation phase, it was reported that the ABC phenomenon was induced by the second dose of a PEGylated liposome, but not of a liposome lacking a PEG-coating (23). This indicates that PEG is essential for the nanocarrier to recognize the antibody in the effectuation phase. In this study, the ABC phenomenon was not observed after repeated injections of the Gd-micelle at different doses and time intervals. This ABC failure of Gd-micelle may be caused by the failure for the production of biological material in the induction phase (data not shown) or/and for the recognization by the antibody in the effectuation phase. Even if the first injection was of empty liposome, the second injection of the Gd-micelle did not produce the ABC phenomenon either. This suggests that the antibody produced by the empty liposome in the induction phase is not recognized by the PEG moiety of the Gd-micelle. Therefore, not only PEG, but also other factors such as structure and hydrophobic character affect recognition.

For the induction phase, the ABC phenomenon was not observed when the amount of PEGylated lipid of liposomes in the first injection was more than 10 mol% (7,8). We have previously reported the accelerated clearance of [^{3}H]-labeled PEGylated liposomes in mice pre-administered empty PEG-PBLA polymeric micelles (16). Furthermore, repeated

injections of PEG-PLA nanoparticles also produced the ABC phenomenon (12). Hence, the structure and component of nanocarriers has a considerable impact on the induction phase of ABC. From a structural perspective, the Gd-micelle formed through ionic interactions; therefore, it does not have any hydrophobic part (Fig. 1). In contrast, the PEG-PBLA micelle is composed of both a hydrophilic part, PEG, and a hydrophobic part, PBLA. Similarly, PEGylated liposomes possess a hydrophilic PEG chain and a hydrophobic bilayer membrane. The immunogenicity of an antigen can be affected by factors such as the physical and chemical properties of the antigen, its dose, and so on (25). The reasons why the Gd-micelle evaded the ABC phenomenon have not yet been elucidated at the present stage. The absence of a hydrophobic part may be a key for this elucidation because the other ABC-phenomenon-positive PEG-based carrier systems possess hydrophobic part in a hydrophobic inner core for polymeric micelles and in a lipid bilayer for PEG-liposomes. We are currently investigating the ABC phenomenon induced by other kinds of polymeric micelles and nanoparticles. It is hoped that these experiments will provide more evidence for the mechanism of the ABC phenomenon.

CONCLUSIONS

The Gd-micelle did not induce ABC following its pre-administration at various doses and time intervals. In contrast, the Gd-liposome induced the phenomenon when it or an empty PEGylated liposome, but not the $PEG_{500,000}$ macromolecule or PEG_{2000}-DSPE, was pre-administered. ABC-phenomenon-positive PEG-based carrier systems possess a hydrophobic part in a hydrophobic inner core for polymeric micelles and in a lipid bilayer for PEG-liposomes. The absence of a hydrophobic part of Gd-micelle may be a key factor for not producing the ABC phenomenon.

ACKNOWLEDGMENTS

This study was supported by the Ministry of Health, Labour, and Welfare of Japan. We also acknowledge the support from the Program for Promoting the Establishment of Strategic Research Centers, Special Coordination Funds for Promoting Science and Technology and the Ministry of Education, Culture, Sports, Science and Technology of Japan.

REFERENCES

1. Allen TM, Hansen C, Martin F, Redemann C, Yau-Young A. Liposomes containing synthetic lipid derivatives of poly(ethylene glycol) show prolonged circulation half-lives *in vivo*. Biochim Biophys Acta. 1991;1066:29–36.
2. Woodle MC, Lasic DD. Sterically stabilized liposomes. Biochim Biophys Acta. 1992;1113:171–99.
3. Lasic DD, Martin FJ, Gabizon A, Huang SK, Papahadjopoulos D. Sterically stabilized liposomes: a hypothesis on the molecular origin of the extended circulation times. Biochim Biophys Acta. 1991;1070:187–92.
4. Torchilin VP, Omelyanenko VG, Papisov MI, Bogdanov AA Jr, Trubetskoy VS, Herron JN, *et al*. Poly(ethylene glycol) on the liposome surface: on the mechanism of polymer-coated liposome longevity. Biochim Biophys Acta. 1994;1195:11–20.
5. Dams ET, Laverman P, Oyen WJ, Storm G, Scherphof GL, van Der Meer JW, *et al*. Accelerated blood clearance and altered biodistribution of repeated injections of sterically stabilized liposomes. J Pharmacol Exp Ther. 2000;292:1071–9.
6. Laverman P, Carstens MG, Boerman OC, Dams ET, Oyen WJ, van Rooijen N, *et al*. Factors affecting the accelerated blood clearance of polyethylene glycol-liposomes upon repeated injection. J Pharmacol Exp Ther. 2001;298:607–12.
7. Ishida T, Ichikawa T, Ichihara M, Sadzuka Y, Kiwada H. Effect of the physicochemical properties of initially injected liposomes on the clearance of subsequently injected PEGylated liposomes in mice. J Control Release. 2004;95:403–12.
8. Ishida T, Harada M, Wang XY, Ichihara M, Irimura K, Kiwada H. Accelerated blood clearance of PEGylated liposomes following preceding liposome injection: effects of lipid dose and PEG surface-density and chain length of the first-dose liposomes. J Control Release. 2005;105:305–17.
9. Ishida T, Kiwada H. Accelerated blood clearance (ABC) phenomenon upon repeated injection of PEGylated liposomes. Int J Pharm. 2008;354:56–62.
10. Judge A, McClintock K, Phelps JR, Maclachlan I. Hypersensitivity and loss of disease site targeting caused by antibody responses to PEGylated liposomes. Mol Ther. 2006;13:328–37.
11. Semple SC, Harasym TO, Clow KA, Ansell SM, Klimuk SK, Hope MJ. Immunogenicity and rapid blood clearance of liposomes containing polyethylene glycol-lipid conjugates and nucleic acid. J Pharmacol Exp Ther. 2005;312:1020–6.
12. Lu W, Wan J, She ZJ, Jiang XG. Brain delivery property and accelerated blood clearance of cationic albumin conjugated pegylated nanoparticle. J Control Release. 2007;118:38–53.
13. Gabizon A, Isacson R, Rosengarten O, Tzemach D, Shmeeda H, Sapir R. An open-label study to evaluate dose and cycle dependence of the pharmacokinetics of pegylated liposomal doxorubicin. Cancer Chemother Pharmacol. 2008;61:695–702.
14. Kakizawa Y, Kataoka K. Block copolymer micelles for delivery of gene and related compounds. Adv Drug Deliv Rev. 2002;54:203–22.
15. Yokoyama M, Okano T, Sakurai Y, Ekimoto H, Shibazaki C, Kataoka K. Toxicity and antitumor activity against solid tumors of micelle-forming polymeric anticancer drug and its extremely long circulation in blood. Cancer Res. 1991;51:3229–36.
16. Koide H, Asai T, Hatanaka K, Urakami T, Ishii T, Kenjo E, *et al*. Particle size-dependent triggering of accelerated blood clearance phenomenon. Int J Pharm. 2008;362:197–200.
17. Lin SP, Brown JJ. MR contrast agents: physical and pharmacologic basics. J Magn Reson Imaging. 2007;25:884–99.
18. Mulder WJ, Strijkers GJ, van Tilborg GA, Griffioen AW, Nicolay K. Lipid-based nanoparticles for contrast-enhanced MRI and molecular imaging. NMR Biomed. 2006;19:142–64.
19. Shiraishi K, Kawano K, Minowa T, Maitani Y, Yokoyama M. Preparation and in vivo imaging of PEG-poly(L-lysine)-based polymeric micelle MRI contrast agents. J Control Release. 2009;136:14–20.
20. Nakamura E, Makino K, Okano T, Yamamoto T, Yokoyama M. A polymeric micelle MRI contrast agent with changeable relaxivity. J Control Release. 2006;114:325–33.
21. Wang XY, Ishida T, Ichihara M, Kiwada H. Influence of the physicochemical properties of liposomes on the accelerated blood clearance phenomenon in rats. J Control Release. 2005;104:91–102.
22. Ishida T, Ichihara M, Wang XY, Yamamoto K, Kimura J, Majima E, *et al*. Injection of PEGylated liposomes in rats elicits PEG-specific IgM, which is responsible for rapid elimination of a second dose of PEGylated liposomes. J Control Release. 2006;112:15–25.
23. Wang XY, Ishida T, Kiwada H. Anti-PEG IgM elicited by injection of liposomes is involved in the enhanced blood clearance of a subsequent dose of PEGylated liposomes. J Control Release. 2007;119:236–44.
24. Sroda K, Rydlewski J, Langner M, Kozubek A, Grzybek M, Sikorski AF. Repeated injections of PEG-PE liposomes generate anti-PEG antibodies. Cell Mol Biol Lett. 2005;10:37–47.
25. Abbas AK, Lichtman AH, Pober JS. Cellular and molecular immunology. Philadelphia: Saunder; 1991.

British Journal of Cancer (2009) 101, 1884–1890
© 2009 Cancer Research UK All rights reserved 0007 – 0920/09 $32.00
www.bjcancer.com

Increase in tumour permeability following TGF-β type I receptor-inhibitor treatment observed by dynamic contrast-enhanced MRI

T Minowa[1], K Kawano[1], H Kuribayashi[2], K Shiraishi[3], T Sugino[4], Y Hattori[1], M Yokoyama[3] and Y Maitani[*,1]

[1]Institute of Medicinal Chemistry, Hoshi University, Ebara 2-4-41, Shinagawa, Tokyo 142-8501, Japan; [2]Varian Technologies Japan Limited, Shibaura 4-16-36, Minato, Tokyo 108-0023, Japan; [3]Kanagawa Academy of Science and Technology, Sakado 3-2-1, Takatsu, Kawasaki, Kanagawa 213-0012, Japan; [4]Department of Basic Pathology, Fukushima Medical University, Hikariga-oka 1, Fukushima 960-1295, Japan

BACKGROUND: To enhance the success rate of nanocarrier-mediated chemotherapy combined with an anti-angiogenic agent, it is crucial to identify parameters for tumour vasculature that can predict a response to the treatment of the anti-angiogenic agent.

METHODS: To apply transforming growth factor (TGF)-β type I receptor (TβR-I) inhibitor, A-83-01, to combined therapy, dynamic contrast-enhanced magnetic resonance imaging (DCE-MRI) was carried out in mice bearing colon 26 cells using gadolinium (Gd)-DTPA and for its liposomal formulation to evaluate changes in tumour microvasculature following A-83-01. Tumour vascular parameters from DCE-MRI were compared with histological assessment and *apparent diffusion coefficient* of water in tumour generated by diffusion-weighted MRI.

RESULTS: Contrary to evaluations reported for anti-angiogenic agents, A-83-01 treatment increased the initial area under the Gd concentration–time curve ($IAUGC_{60}$), volume transfer constant (K^{trans}) and fractional plasma volume (v_p) significantly within 24 h, that was positively related to α-smooth muscle actin-positive pericyte coverage and tumour cell proliferation, and was correlated inversely with the *apparent diffusion coefficient*. The vascular function of the tumour improved by A-83-01 treatment was well assessed on post-liposomal Gd-DTPA-enhanced MR images, which predicted delivery of a liposomal drug to the tumour.

CONCLUSION: These findings suggest that DCE-MRI and, in particular, K^{trans} and v_p quantitation, provide important additional information about tumour vasculature by A-83-01 treatment.

British Journal of Cancer (2009) **101**, 1884–1890. doi:10.1038/sj.bjc.6605367 www.bjcancer.com
Published online 3 November 2009
© 2009 Cancer Research UK

Keywords: MRI; liposome; angiogenesis; TGF-β inhibitor; contrast agent; tumour

Molecular Diagnostics

The success of chemotherapeutic agents with solid tumours is critically dependant on the access that these agents have to the tumours via the so-called 'leaky vasculature'. In particular, tumour vasculature is crucial for the delivery of drugs encapsulated in nanocarriers (Matsumura and Maeda, 1986). Anti-angiogenesis effects are known to change the tumour vasculature; therefore, this technique has been already applied to combined therapy. Bevacizumab, an anti-vascular endothelial growth factor (VEGF) antibody, was developed for blocking angiogenesis and it is clinically used with other drugs to improve the efficiency of chemotherapy.

The roles of transforming growth factor (TGF)-β in cancer biology are complex; TGF-β can suppress or promote tumour growth depending on the type of cancer. Small molecule TGF-β type I receptor (TβR-I) inhibitor has a wide variety of effects (Jakowlew, 2006; Tsuchida *et al*, 2006). The TβR-I inhibitor LY364947 was reported to increase the accumulation of an anti-cancer drug encapsulated in nanocarriers by changing the micro-environmental vasculature (Kano *et al*, 2007). The TβR-I inhibitor A-83-01 is one of more potent inhibitors of TβR-I kinase/activin receptor-like kinase (ALK)-5 (IC_{50} = 12 nM) (Tojo *et al*, 2005) than a previously described ALK-5 inhibitors including LY364947 (IC_{50} = 59 nM) (Li *et al*, 2006), although the *in vivo* effect has not been made known. To estimate the tumour state after treatment with TβR-I inhibitor is important to determine an administration schedule for TβR-I inhibitor-combined therapy. However, it is difficult to rationally determine whether tumour blood vessels are amenable to nanocarrier-mediated therapy in an individualised manner.

Dynamic contrast-enhanced magnetic resonance imaging (DCE-MRI) is one of the evaluation methods of anti-angiogenic agents, such as anti-VEGF antibody and tyrosine kinase inhibitor, clinically (Morgan *et al*, 2003; O'Connor *et al*, 2007) and preclinically (Marzola *et al*, 2004; Nakamura *et al*, 2006; Bradley *et al*, 2009), by calculating pharmacokinetic parameters, including fractional plasma volume (v_p) and the volume transfer constant (K^{trans}) from the enhancement of tumour signal intensity by gadolinium (Gd) contrast agent (Tozer, 2003; Kiessling *et al*, 2007). To my knowledge, however, there are no reports to evaluate TβR-I inhibitor by DCE-MRI. In clinical studies, small molecular weight contrast agents, Gd chelates, have been used. K^{trans}, the Gd exchange constant between blood and tumour interstitial tissue, depends on the balance between permeability and blood flow. Therefore, the K^{trans} parameter depends on the size of the contrast

*Correspondence: Dr Y Maitani; E-mail: yoshie@hoshi.ac.jp
Received 8 July 2009; revised 2 September 2009; accepted 17 September 2009; published online 3 November 2009

agent. The choice of the optimal contrast agent is considered to be essential for a successful characterisation of tumour angiogenesis. As macromolecule contrast media show lower permeability than Gd chelates, it is useful for permeability change monitoring in tumour vasculature (Daldrup-Link *et al*, 2004; Turetschek *et al*, 2004); Liposomes are self-closed colloidal particles in which bilayer membranes composed from self-aggregated lipid molecules encapsulate a fraction of the medium. Liposomes have been used as drug carriers for anticancer drugs such as Doxil. For this reason, liposomal Gd has a substantial potential to detect permeability-limited conditions. There are still no reports on the use of liposomes as a DCE-MRI contrast agent. Furthermore, liposomal contrast agents to evaluate nanocarrier behaviour in tumour directly will be a hopeful method of examination for combination therapy.

Thus, the purpose of this study was to evaluate changes in tumour vasculature as parameters using DCE-MRI to monitor responses in mice following A-83-01 administration. In addition to DCE-MRI, diffusion-weighted imaging was used to estimate *the apparent diffusion coefficient* of tissue water (Koh and Padhani, 2006; Patterson *et al*, 2008). TβR-I inhibitor activity was also evaluated in representative experiments through tumour vascularity, the proportion of endothelial cells associated with pericytes, and microvessel density from histological slices.

MATERIALS AND METHODS

Animals

All animal experiments were carried out in accordance with the guidelines of the Guiding Principles for the Care and Use of Laboratory Animals of Hoshi University. Colon 26 cells (1×10^6) were inoculated subcutaneously into the right back at the side of the heart in CDF1 female mice (6-weeks old, Sankyo Labo Service, Tokyo, Japan). When the tumour size reached approximately 100 mm^3, A-83-01 (Sigma Chemical, St. Louis, MO, USA) (Supplementary Figure S1A) dissolved in DMSO/saline=3 out of 2 (v/v) was injected intraperitoneally. The tail vein was catheterised post-injection of contrast agent during the DCE-MRI experiment. Mice were anaesthetised with 1.5% isoflurane (Abbott Japan, Tokyo, Japan) throughout the MRI experiment during their insertion into a 9.4T vertical type MRI (Varian, Palo Alto, CA, USA). For a single treatment of A-83-01, mice (N=4) were injected with A-83-01 at a dose of 1 mg kg^{-1} at '0 h' (Supplementary Figure S1B). In this experiment, 0 h was the time of the first A-83-01 intraperitoneal injection and the number of hours represents time after the first injection of A-83-01. For repeated treatment, mice (N=4) were injected with A-83-01 at 0 and 21 h at the same dose as for the single treatment.

Preparation of liposomal Gd-DTPA

For the preparation of liposomal Gd-DTPA (Gd-L), mixture of egg phosphatidylcholine (Q.P. Company, Tokyo, Japan), cholesterol (Wako Pure Chemical Industries, Osaka, Japan), and polyethyleneglycol 2000-distearoyl phosphatidylethanolamine (NOF, Tokyo, Japan) in a molar ratio of 5:2:0.35 was dissolved in ethanol at 60°C, hydrated with Gd-DTPA (Magnevist, Bayer-Schering Pharma AG, Berlin, Germany), stirred, and evaporated under a vacuum to remove ethanol. This mixture was exposed to ultrasound until the particle diameter was about 120 nm, followed by exhausted dialysis against phosphate buffered saline (pH 7.4) solution. The particle size of the liposomes was determined at 25°C using an ELS-Z2 instrument (Otsuka Electronics, Tokyo, Japan). The Gd concentration was determined using *inductively coupled plasma* with an SPS7800 apparatus (SII NanoTechnology, Tokyo, Japan). T^1 relaxation times of Gd-L and Gd-DTPA were measured over the concentration range of 0–0.25 mM Gd at 9.4 T_1 at room temperature. Relaxivity (R^1) was then determined from the slope of the linear regression fits of $1/T_1$ vs the Gd concentration: $1/T_1 = R_1 \times [Gd] + 1/T_{10}$, where T_{10} represents T_1 of 0 mM Gd solution. R_1 of Gd-L was 4.48 $mM^{-1}s^{-1}$, which was similar to that of Gd-DTPA (4.39 $mM^{-1}s^{-1}$).

MRI

Apparent diffusion coefficient was estimated and mapped from *diffusion-weighted imaging* using the following parameters: repetition time (TR)=2000 ms, echo time (TE)=45 ms, slice thickness 3 mm, 64 × 64 data matrix, axial orientation, and field-of-view of 3 × 3 cm^2. Three slices through the centre of the tumour were acquired. Diffusion gradients equivalent to b-values of 0, 200, 400, and 800 s mm^{-2} were employed using gradient pulse widths of $\delta = 7$ ms and $\Delta = 20$ ms.

Dynamic contrast-enhanced magnetic resonance imaging was carried out with Gd-DTPA and Gd-L before ('pre') and after treatment in each animal. With the use of Gd Gd-L, injected lipids containing Gd-L were retained in the tumour; therefore, different mice were used to compare pretreatment with treatment of A-83-01. Before DCE-MRI high spatial resolution, two-dimensional T_2-weighted spin–echo axial images were acquired to detect the tumour position. Pre-contrast tumour T_1 was determined using an inversion recovery-prepared spoiled gradient-recalled echo (SPGR) sequence. The inversion-recovery was carried out using a 180° hard RF pulse followed by a gradient crusher pulse. Inversion times were 0.2, 0.4, 0.8, 1.4, 2, and 3 s. The other MRI parameters were; TE=3 ms, field-of-view=3 × 3 cm^2, slice thickness=4 mm, and matrix size=64 × 64. Both RF and gradient spoilers were applied. In DCE-MRI acquisition, it was applied repeatedly to acquire the axial slice SPGR images through the tumour and left ventricle with a second temporal resolution over 6 min: TR=7.8125 ms, TE=2.06 ms, matrix resolution=64 × 64, field-of-view=3 × 3 cm^2, slice thickness=4 mm, flip angle=30°, number of slices=1, and two signal averages. Approximately 20 s of baseline DCE-MRI images were acquired. Gd-DTPA or Gd-L was administered at 20 μl g^{-1} (0.1 mmol Gd kg^{-1}) as a bolus with heparinized saline (total volume ~0.4 ml) via manual injection over 2–3 s.

Quantitative evaluation of MRI

Tumour regions-of-interest (ROI) covering the whole tumour was segmented on the T_2-weighted axial images, using ImageJ software (NIH, Bethesda, MD, USA), and the tumour ROI was transferred to the *apparent diffusion coefficient* map calculated from *diffusion-weighted imagings*.

A T_1 map of tumour was prepared by the imaging of the inversion-recovery method to quantitate tumour Gd concentrations. The concentration of Gd at each imaging time point in each voxel was estimated using the formula Bradley *et al* (2009) used. T_1 in blood plasma at 9.4 T was 2.2 s, as reported previously (Tsekos *et al*, 1998) and T_1 in tumour was from the T_1 map. $1/T_1$ (t) was calculated for every time point for the blood and tumour Gd concentrations. The initial area under the Gd concentration–time curve over 60 s ($IAUGC_{60}$) was calculated. The tumour haemodynamic parameters K^{trans} and v_p were calculated using a two-compartment model (Ewing *et al*, 2003). The plasma concentration over time was calculated from the left ventricle data, which were averaged for all mice in the Gd-DTPA and Gd-L groups for this value.

Histological and immunohistochemical analysis

For the histological assessment of A-83-01 effects on tumour vasculature, tumour sections were observed at 24 h after repeated injection of A-83-01. Each of four tumours from A-83-01 treated

© 2009 Cancer Research UK

and untreated mice was resected and fixed with 10% formalin. Paraffin-embedded samples were sliced into 3 μM sections for *hematoxylin and eosin* staining and immunostaining. Antibodies against α-smooth muscle actin (SMA) (DAKO, Glostrup, Denmark) were used to identify the pericyte and anti-CD31 (Abcam, MA, USA, USA), endothelial cell marker and anti-Ki67 (Labvision, Fremont, CA, USA) antibodies to recognise the growth state cells (G1, S, and M phase). Vascular areas within the tumours were measured as the index of tumour vascularity by stained with anti-CD31. Five fields of tumour sections were analysed at low magnification using a computerised image analyser (Image-Pro Plus, Media Cybernetics, MA, USA). The ratio of vessel area against tumour area without necrosis was calculated.

Statistical analysis

Values were expressed as the mean ± s.d. A two-tailed Student's *t*-test was used comparison between the pre- and post-treatment groups. ANOVA analysis, followed by Dunnett's test, was used for multi-group comparisons. Pearson's correlation coefficients were used for determination between a significant positive and negative relationship. Correlations between 0.4 and 0.6 were considered moderate, whereas correlations from 0.7 to 1.0 were considered strong. Significant differences were accepted when the *P*-value was below 0.05.

RESULTS

Figure 1A shows change of the Gd concentrations in DCE-MRI acquisition using Gd-DTPA at pretreatment, at 3-h, and 24-h post-injection of A-83-01. A progressive accumulation of Gd in the tumour was observed during the first 60 s followed by a plateau phase. The group treated with a single injection of A-83-01 showed the highest accumulation at 3 h post-injection of A-83-01 (1.7-fold the $IAUGC_{60}$, Figure 1B) associated with a larger s.d., and a similar level to those with pretreatment at 24 h (0.9-fold the $IAUGC_{60}$). At 24 h after repeated injection, the tumour accumulation increased a similar level to that at 3 h after the single injection (1.8-fold the $IAUGC_{60}$). Next, we observed changes of the tumour vasculature repeat-treated by A-83-01 using Gd-L. The Gd concentration in DCE-MRI acquisition of untreated mice was very low (Figure 1C). The Gd concentration with Gd-L in repeat-treated mice increased during the first 200 s, and reached the same plateau value as with that of the Gd-DTPA repeat-treated mice. Eventually the repeated A-83-01 treatment increased 3.8-fold the $IAUGC_{60}$ of Gd-L (Figure 1D), indicating a dramatic improvement in liposomal contrast agent delivery to the tumour.

From the data obtained above, v_p and K^{trans} values were calculated (Figure 2). With Gd-DTPA at 3 h after the single treatment, v_p and K^{trans} were high values accompanied with great variability, whereas at 24 h, v_p and K^{trans} were similar to those of the respective pretreatment values, suggesting that A-83-01 induced a transient change in the vasculature at around 3 h. On the other hand, at 24 h after repeated treatment, all mice showed increased v_p and K^{trans} with Gd-DTPA ($P<0.05$) and Gd-L. At 3 h after the first treatment, v_p and K^{trans} did not show significantly elevated values with Gd-DTPA, therefore, it can be concluded that the repeated administration schedule changed the tumour state positively for better liposomal contrast-agent distribution. The most characteristic point of the v_p and K^{trans} changes was the large dispersion of v_p and K^{trans} values after repeated A-83-01 treatments with the use of Gd-L. The diversity of local permeability of treated tumours may lead to large

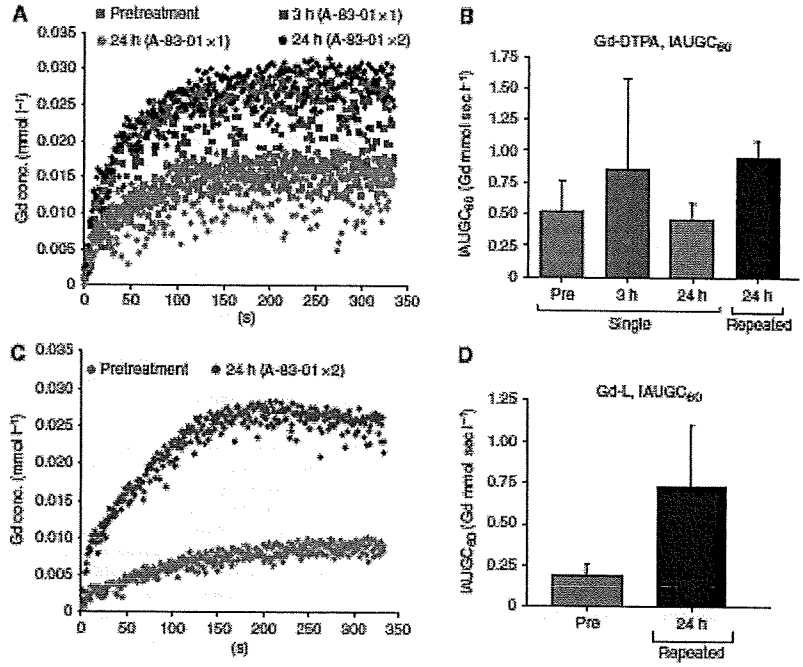

Figure 1 Mean gadolinium (Gd) uptake curves from regions-of-interest (ROI) over the whole tumour before (pre) and at different time points after (post) intraperitoneal A-83-01 injection with Gd-DTPA (**A**) and Gd-L (**C**), and $IAUGC60_{0-60}$ with Gd-DTPA (**B**) and Gd-L (**D**). Data points (**B**, **D**) indicate mean ± s.d. ($N=3-6$).

© 2009 Cancer Research UK

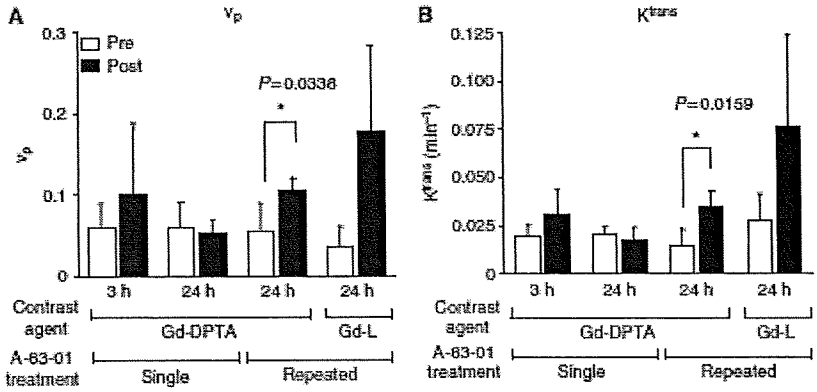

Figure 2 Values of fractional plasma volume (v_p) (**A**) and volume transfer constant (K^{trans}) (**B**) in the tumour before (pre) and at 3 h and 24 h after (post) single or repeated A-83-01 injections using gadolinium (Gd)-DTPA and Gd-L as a contrast agent. Each column represents the mean ± SD (N = 3 to 6).

dispersion of Gd-L. The mouse tumour core showed an increase in the Gd concentration, as shown in Figure 1C, whereas the tumour rim showed a high peak concentration at about 1 min post-injection of Gd-L that then decayed (data not shown). In contrast, Gd-DTPA increased tumour Gd concentration homogeneously. This finding suggests that Gd-L could detect small changes in tumour micro-environments and brought about a big dispersion of v_p and K^{trans} values among treated mice.

Figure 3 shows histological observations of the tumours with or without the repeated A-83-01 treatment. Two distinct changes were observed, although there was no difference in tumour cell shape or necrosis. The first was intra-tumoural bleeding, which was exclusively configured at the periphery of the A-83-01-treated tumours with 200–300 μm width and 100 μm depth (Figure 3A). The bleeding lesions were not accompanied with tissue oedema, suggesting minute rupture of tumour vessels. This means that hyper-permeability had not occurred. The localised bleeding state may correspond to the accumulation site of Gd-L. The second observation was morphological changes of the tumour vasculature. Abnormal blood vessels with irregular dilation were seen in the untreated tumours, whereas the vasculature in A-83-01-treated mice was smaller, and its shape was more round, suggesting the vascular normalisation (Figure 3A). Tumour vascularity, the percentage of vascular area (1.2%) in the treated tumours (post) was not significantly lower than in the untreated tumours (pre, 2.9%, $P > 0.05$), as the change was very diverse within a tumour (Figure 3D). The abnormal tumour vessels were not accompanied with pericytes, which were identified because of SMA reactivity (Figure 3B). It is interesting to note that the normalised vessels in tumours treated with A-83-01 were surrounded by pericytes (Figure 3B). The Ki67 index (58.5%) was significantly higher in the perivascular region of the A-83-01-treated tumours compared with the untreated tumours (41.4%, $P < 0.05$) (Figure 3C, E). These findings suggested that the repeated A-83-01 treatment allowed the recovery of blood flow during 24 h.

In the evaluation of *apparent diffusion coefficient* value, single-treated groups at 3 and 24 h did not show a difference compared with the pretreatment, but the repeat-treated group at 24 h showed a significant difference ($P < 0.01$, Figure 4). Alteration of extra- and intracellular fluid volume balance in repeat-administrated protocol may occur in the tumour because the diffusion rate of intracellular water is 1 order of magnitude smaller than that of the extracellular water (Van Zijl *et al*, 1991; Gass *et al*, 2001).

Next, the relation of DCE-MRI parameters with Gd-DTPA to tumour *apparent diffusion coefficient* was investigated (Figure 5). There was a moderately negative correlation between *the* $IAUGC_{60}$ (Figure 5A), K^{trans} (Figure 5B), v_p, *and apparent diffusion coefficient* (Figure 5C). This suggests that these parameters may be of value in the assessment of tumour behaviour.

DISCUSSION

In this study, effects of a TβR-I inhibitor was firstly evaluated by means of DCE-MRI with Gd-DTPA and Gd-L in mice bearing colon 26 tumours. The effect of A-83-01 exhibited high $IAUGC_{60}$, v_p, and K^{trans} values at 24 h after repeated treatment.

An increase in K^{trans} by the use of Gd-L could conceivably increase the permeability and surface area of the capillary endothelium. The K^{trans} value estimated with Gd-L ($K^{trans} = 0.076 \pm 0.048\,min^{-1}$) after the repeated A-83-01 treatment was higher to that with Gd-DTPA ($K^{trans} = 0.035 \pm 0.009\,min^{-1}$) (Figure 2B). Liposomal contrast agents are promising for characterising the tumour vascularity and the angiogenesis status through DCE-MRI method.

Anti-angiogenic agents such as anti-VEGF antibody and tyrosine kinase inhibitor were reported that decrease both K^{trans} and IAUGC (O'Connor *et al*, 2007; Bradley *et al*, 2008; Bradley *et al*, 2009), and the decrease in K^{trans} in solid tumours is concerned with the anti-tumour effect (Morgan *et al*, 2003; Marzola *et al*, 2004; Nakamura *et al*, 2006; Flaherty *et al*, 2008). In this study, K^{trans}, $IAUGC_{60}$, and v_p were increased significantly 24 h after the A-83-01 treatment. This increase may be explained by different treatment protocols, different tumour models, and the different signal inhibition between anti-angiogenic agent such as kinase inhibitor and TβR-I inhibitor. Similar to A-83-01-treated colon 26 solid tumours, LY364947-treated M109 solid tumours increased $IAUGC_{60}$ at 3 h and recovered fully by 24 h post-injection (Supplementary Figure S2).

It was reported that in a limited situation, anti-angiogenic agents work to deliver more drugs into tumours through the induction of vascular normalisation (Jain, 2001). Untreated colon 26 tumours showed low permeability, in spite of the absence of pericytes or the leaky vessel state (Figure 2B, 3B). The increased K^{trans} and $IAUGC_{60}$ values were related to the increased number of growth state cells around the tumour vessel, and were correlated to the decreased *apparent diffusion coefficient value*. Because of no significant difference in tumour cell shape after treatment (Figure 3A), intra-cellular volume did not change. Decreased *apparent diffusion coefficient*, therefore, reflected a decrease in

© 2009 Cancer Research UK

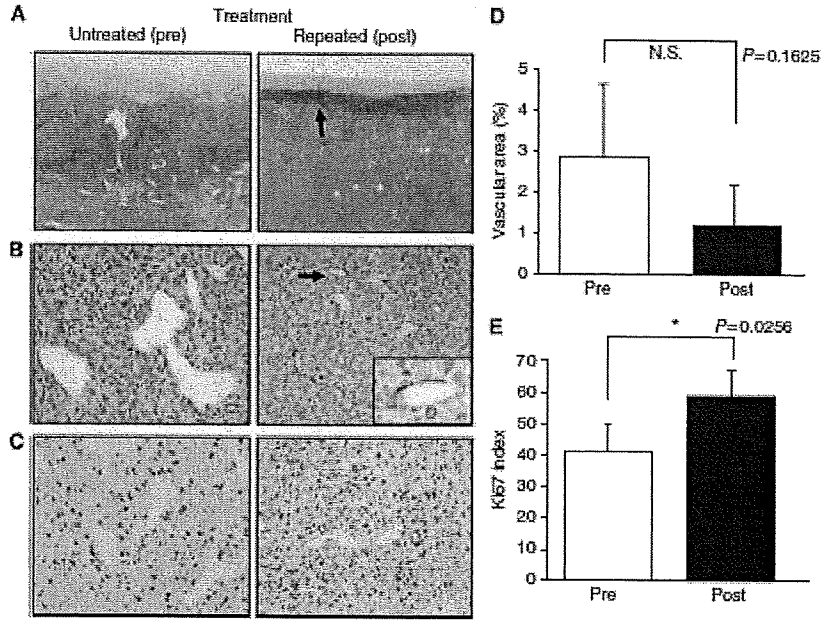

Figure 3 Histological analysis of tumours in untreated (pre) and treated (post) mice 24 h after repeated A-83-01 treatment. (**A**) *Hematoxylin and eosin* staining (× 40). Arrow indicates that zonal bleeding was observed at the periphery of the tumour with A-83-01 treatment. (**B**) Immunostaining with anti-smooth muscle actin (SMA) antibody (× 200 and inset, × 400). Irregularly dilated tumour vessels in untreated mice are not associated with pericytes, whereas the normalized vessels after A-83-01 treatment are surrounded by SMA-positive pericytes (arrow). (**C**) Immunostaining with Ki67. Ki67-positive proliferating tumour cells in the perivascular region are more prominent in the A-83-01 treated tumour than the untreated tumour (× 200). (**D**) Mean percentage of the vascular areas within the tumours as the index of tumour vascularity. (**E**) Ki67 index in perivascular regions of (**C**). Proliferating tumour cells were increased significantly in A-83-01 treated tumours compared with untreated tumours ($P<0.05$). Each column represents the mean ± s.d. ($N=5$).

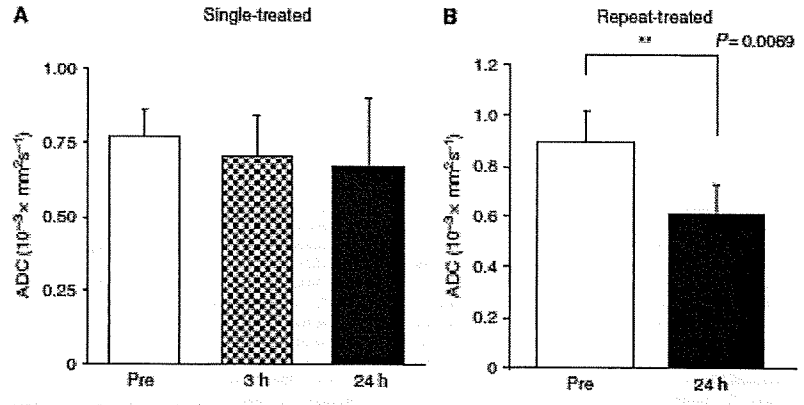

Figure 4 *Apparent diffusion coefficient* of the tumours before (pre) and at different time points after (post) single (**A**) and repeated (**B**) intraperitoneal A-83-01 injection. Repeat-treated tumours showed significant decreases in *apparent diffusion coefficient* compared with pretreatment. Each column represents the mean ± s.d. ($N=4$).

extra-cellular fluid, suggesting that the recovery of delivery may be related to vessel normalisation.

Furthermore, similar to negative correlation between tumour interstitial fluid pressure and permeability of tumour (Haider *et al*, 2007), IAUGC, K^{trans}, and v_p showed a moderate negative correlation to *apparent diffusion coefficient*, suggesting that these parameters may be providing similar information. As *apparent diffusion coefficient* is acquired in clinic widely to detect and diagnose a tumour, it could apply conveniently to examine the permeability of tumour in patients.

Although there is room for improvement, DCE-MRI using liposomal contrast agents such as Gd-L could be an important method to anticipate the extravasation of the liposomal anti-cancer drug during TβR-I inhibitor-combined therapy.

© 2009 Cancer Research UK

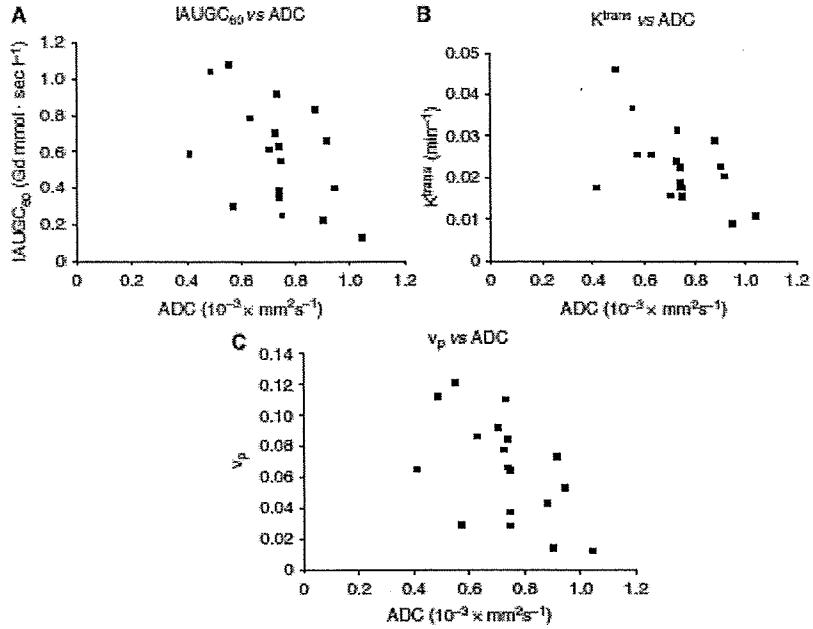

Figure 5 $IAUGC_{60}$, transfer constant volume transfer constant (K^{trans}), and fractional plasma volume (v_p) with gadolinium (Gd)-DTPA *vs* tumour *apparent diffusion coefficient* (ADC). There was a moderately negative correlation between the $IAUGC_{60}$ and ADC ($r=-0.4774$, $P=0.0451$, $N=18$) (**A**), between K^{trans} and ADC ($r=-0.5333$, $P=0.0227$, $N=18$) (**B**), and between v_p and ADC ($r=-0.5253$, $P=0.0252$, $N=18$) (**C**).

In summary, we found that DCE-MRI parameters, K^{trans}, $IAUGC_{60}$, and v_p, were positively related to tumour vasculature by the treatment of A-83-01. Thus, TβR-I inhibitor has the potential to enhance the delivery of liposomal anti-cancer drugs and contrast agents. DCE-MRI forms a capable tool to determine the administration schedule of combination therapy with TβR-I inhibitor by K^{trans} and v_p quantitation.

ACKNOWLEDGEMENTS

This work was supported in part by a grant for research on Regulatory Science of Pharmaceuticals and Medical Devices from the Ministry of Health, Labor and Welfare of Japan and by the Open Research Center Project. Ms Y Taniguchi is acknowledged for providing many helpful comments, and Mr S Kawagoe and Mr T Nakamura for assistance.

REFERENCES

Bradley DP, Tessier JJ, Lacey T, Scott M, Jurgensmeier JM, Odedra R, Mills J, Kilburn L, Wedge SR (2009) Examining the acute effects of cediranib (RECENTIN, AZD2171) treatment in tumor models: a dynamic contrast-enhanced MRI study using gadopentate. *Magn Reson Imaging* 27: 377–384

Bradley DP, Tessier JJ, Checkley D, Kuribayashi H, Waterton JC, Kendrew J, Wedge SR (2008) Effects of AZD2171 and vandetanib (ZD6474, Zactima) on haemodynamic variables in an SW620 human colon tumour model: an investigation using dynamic contrast-enhanced MRI and the rapid clearance blood pool contrast agent, P792 (gadomelitol). *NMR Biomed* 21: 42–52

Daldrup-Link HE, Okuhata Y, Wolfe A, Srivastav S, Oie S, Ferrara N, Cohen RL, Shames DM, Brasch RC (2004) Decrease in tumor apparent permeability-surface area product to a MRI macromolecular contrast medium following angiogenesis inhibition with correlations to cytotoxic drug accumulation. *Microcirculation* 11: 387–396

Ewing JR, Knight RA, Nagaraja TN, Yee JS, Nagesh V, Whitton PA, Li L, Fenstermacher JD (2003) Patlak plots of Gd-DTPA MRI data yield blood-brain transfer constants concordant with those of 14C-sucrose in areas of blood-brain opening. *Magn Reson Med* 50: 283–292

Flaherty KT, Rosen MA, Heitjan DF, Gallagher ML, Schwartz B, Schnall MD, O'Dwyer PJ (2008) Pilot study of DCE-MRI to predict progression-free survival with sorafenib therapy in renal cell carcinoma. *Cancer Biol Ther* 7: 496–501

Gass A, Niendorf T, Hirsch JG (2001) Acute and chronic changes of the apparent diffusion coefficient in neurological disorders–biophysical mechanisms and possible underlying histopathology. *J Neurol Sci* 186: 515–523

Haider MA, Sitartchouk I, Roberts TP, Fyles A, Hashmi AT, Milosevic M (2007) Correlations between dynamic contrast-enhanced magnetic resonance imaging-derived measures of tumor microvasculature and interstitial fluid pressure in patients with cervical cancer. *J Magn Reson Imaging* 25: 153–159

Jain RK (2001) Normalizing tumor vasculature with anti-angiogenic therapy: a new paradigm for combination therapy. *Nat Med* 7: 987–989

Jakowlew SB (2006) Transforming growth factor-beta in cancer and metastasis. *Cancer Metastasis Rev* 25: 435–457

Kano MR, Bae Y, Iwata C, Morishita Y, Yashiro M, Oka M, Fujii T, Komuro A, Kiyono K, Kaminishi M, Hirakawa K, Ouchi Y, Nishiyama N, Kataoka K, Miyazono K (2007) Improvement of cancer-targeting therapy, using nanocarriers for intractable solid tumors by inhibition of TGF-beta signaling. *Proc Natl Acad Sci USA* 104: 3460–3465

Kiessling F, Morgenstern B, Zhang C (2007) Contrast agents and applications to assess tumor angiogenesis *in vivo* by magnetic resonance imaging. *Curr Med Chem* 14: 77–91

© 2009 Cancer Research UK

Koh DM, Padhani AR (2006) Diffusion-weighted MRI: a new functional clinical technique for tumour imaging. *Br J Radiol* 79: 633–635

Li HY, Wang Y, Heap CR, King CH, Mundla SR, Voss M, Clawson DK, Yan L, Campbell RM, Anderson BD, Wagner JR, Britt K, Lu KX, McMillen WT, Yingling JM (2006) Dihydropyrrolopyrazole transforming growth factor-beta type I receptor kinase domain inhibitors: a novel benzimidazole series with selectivity versus transforming growth factor-beta type II receptor kinase and mixed lineage kinase-7. *J Med Chem* 49: 2138–2142

Manzola P, Degrassi A, Calderan L, Farace P, Crescimanno C, Nicolato E, Giusti A, Pesenti E, Terron A, Sbarbati A, Abrams T, Murray L, Osculati F (2004) In vivo assessment of antiangiogenic activity of SU6668 in an experimental colon carcinoma model. *Clin Cancer Res* 10: 739–750

Matsumura Y, Maeda H (1986) A new concept for macromolecular therapeutics in cancer chemotherapy: mechanism of tumoritropic accumulation of proteins and the antitumor agent smancs. *Cancer Res* 46: 6387–6392

Morgan B, Thomas AL, Drevs J, Hennig J, Buchert M, Jivan A, Horsfield MA, Mross K, Ball HA, Lee L, Mietlowski W, Fuxuis S, Unger C, O'Byrne K, Henry A, Cherryman GR, Laurent D, Dugan M, Marme D, Steward WP (2003) Dynamic contrast-enhanced magnetic resonance imaging as a biomarker for the pharmacological response of PTK787/ZK 222584, an inhibitor of the vascular endothelial growth factor receptor tyrosine kinases, in patients with advanced colorectal cancer and liver metastases: results from two phase I studies. *J Clin Oncol* 21: 3955–3964

Nakamura K, Taguchi E, Miura T, Yamamoto A, Takahashi K, Bichat F, Guilbaud N, Hasegawa K, Kubo K, Fujiwara Y, Suzuki R, Kubo K, Shibuya M, Isae T (2006) KRN951, a highly potent inhibitor of vascular endothelial growth factor receptor tyrosine kinases, has antitumor activities and affects functional vascular properties. *Cancer Res* 66: 9134–9142

O'Connor JP, Jackson A, Parker GJ, Jayson GC (2007) DCE-MRI biomarkers in the clinical evaluation of antiangiogenic and vascular disrupting agents. *Br J Cancer* 96: 189–195

Patterson DM, Padhani AR, Collins DJ (2008) Technology insight: water diffusion MRI–a potential new biomarker of response to cancer therapy. *Nat Clin Pract Oncol* 5: 220–233

Tojo M, Hamashima Y, Hanyu A, Kajimoto T, Saitoh M, Miyazono K, Node M, Imamura T (2005) The ALK-5 inhibitor A-83-01 inhibits Smad signaling and epithelial-to-mesenchymal transition by transforming growth factor-beta. *Cancer Sci* 96: 791–800

Tozer GM (2003) Measuring tumour vascular response to antivascular and antiangiogenic drugs. *Br J Radiol* 76: S23–S35

Tsekos NV, Zhang F, Merkle H, Nagayama M, Iadecola C, Kim SG (1998) Quantitative measurements of cerebral blood flow in rats using the FAIR technique: correlation with previous iodoantipyrine autoradiographic studies. *Magn Reson Med* 39: 564–573

Tsuchida K, Sunada Y, Noji S, Murakami T, Uezumi A, Nakatani M (2006) Inhibitors of the TGF-beta superfamily and their clinical applications. *Mini Rev Med Chem* 6: 1255–1261

Turetschek K, Preda A, Novikov V, Brasch RC, Weinmann HJ, Wunderbaldinger P, Roberts TP (2004) Tumor microvascular changes in antiangiogenic treatment: assessment by magnetic resonance contrast media of different molecular weights. *J Magn Reson Imaging* 20: 138–144

Van Zijl PC, Moonen CT, Faustino P, Pekar J, Kaplan O, Cohen JS (1991) Complete separation of intracellular and extracellular information in NMR spectra of perfused cells by diffusion-weighted spectroscopy. *Proc Natl Acad Sci USA* 88: 3228–3232

© 2009 Cancer Research UK

Journal of Controlled Release 136 (2009) 14–20

Contents lists available at ScienceDirect

Journal of Controlled Release

journal homepage: www.elsevier.com/locate/jconrel

Preparation and in vivo imaging of PEG-poly(L-lysine)-based polymeric micelle MRI contrast agents

Kouichi Shiraishi [a], Kumi Kawano [b], Takuya Minowa [b], Yoshie Maitani [b], Masayuki Yokoyama [a,*]

[a] Kanagawa Academy of Science and Technology, Yokoyama "Nano-medical Polymers" Project, KSP East 404, Sakado 3-2-1, Takatsu-ku, Kawasaki, Kanagawa 213-0012, Japan
[b] Institute of Medicinal Chemistry, Hoshi University, 2-4-41 Ebara, Shinagawa-ku, Tokyo 142-8501, Japan

ARTICLE INFO

Article history:
Received 24 October 2008
Accepted 17 January 2009
Available online 23 January 2009

Keywords:
Polymeric micelle
MRI contrast agent
Long circulation
Tumor imaging
Poly(ethylene glycol)-b-poly(L-lysine)

ABSTRACT

A polymeric micelle drug carrier system was applied to the targeting of an MRI (magnetic resonance imaging) contrast agent. A block copolymer, PEG-*b*-poly(L-lysine), was used for conjugation of gadolinium ions through chelating moieties, DOTA. The DOTA moieties were successfully conjugated to all primary amine groups of the lysine residues. The obtained block copolymer, PEG-*b*-poly(L-lysine-DOTA), formed a polymeric micelle. The polymeric micelle structure was maintained even after partial gadolinium chelation (~40%) to the DOTA moieties. The prepared polymeric micelle MRI contrast agent was injected into a mouse tail vein at a dose of 0.05 mmol Gd/kg. The polymeric micelle-based MRI contrast agent exhibited stable blood circulation. A considerable amount (6.1 ± 0.3% of ID/g of the polymeric micelle) was found to accumulate at solid tumors 24 h after intravenous injection by means of the EPR effect. An MRI analysis revealed that the signal intensity of the tumor was enhanced 2.0-fold by the use of this contrast agent.

© 2009 Elsevier B.V. All rights reserved.

1. Introduction

Various types of nano-sized drug carriers including linear synthetic polymers, dendrimers, proteins, liposomes, and polymeric micelles have been investigated for anti-cancer drug targeting to solid tumor sites for improvements in cancer chemotherapy [1,2]. Among these nano-sized carrier systems, polymeric micelles have been studied with a focus on encapsulation of hydrophobic drugs [3]. Most typically, polymeric micelles are constituted of block copolymers having a hydrophilic chain such as PEG and a hydrophobic chain. The hydrophobic chain can form a hydrophobic inner core that incorporates hydrophobic drugs. A strong advantage of the polymeric micelles is their high structural stability in the bloodstream and their very small size, being in a range of 10–100 nm. This size range is preferable for the passive targeting of solid tumors by means of the EPR (enhanced permeability and retention) effect [3]. Successful tumor-targeting-carrier systems include the adriamycin-incorporated polymeric micelle system [1], which involves a metal complex drug-incorporated (e.g., cisplatin-incorporated) polymeric system [4–6].

The recent study reported that several nano-sized-carrier system and, in particular, diagnostic imaging agents rest on drug-targeting methodology. Magnetic resonance imaging (MRI) is a non-invasive imaging modality for diagnosis. Owing to rapid developments in temporal and spatial resolution, the value of MRI has grown greater in recent decades. Nowadays, much attention is given to MRI contrast agents both of low molecular weight and of macromolecule status for their ability to improve MRI signals.

Paramagnetic metal complexes, such as the gadolinium (III) ion–DTPA complex, are widely used in clinical diagnosis. Such gadolinium complexes enhance T_1-weighted images by shortening the T_1-relaxation time of the water protons. Linear polymers such as dextran [7,8], poly(L-lysine) [9,10], poly(glutamic acid) [11–13], and poly[N-(2-hydroxypropyl)methacrylamide] [14] have been investigated as possible for carriers of the gadolinium complexes. Dendrimers, which possess well-defined structures and accurate molecular weights, have also attracted much attention as carriers of MRI contrast agents because dendrimers' biodistribution were depend on the generations [15–17].

Polymeric micelle-based MRI contrast agents also have a potential as MRI contrast agents. Because the polymeric micelle is an associate of many block copolymer chains, block copolymers with well-controlled molecular weight can be excreted through kidney filtration after dissociation of the polymeric micelles into block copolymer chains. Therefore, a low risk of chronic toxicity is expected to present itself and is expected to stem from polymeric micelles' complete excretion over a long time period. On the other hand, polymeric micelles can exhibit a preferential pharmacokinetic profile in a defined time period required for the targeting of tumors. In a previous report, we prepared a polyion complex micelle from charged block copolymers and counter ionic polymers [18]. This polymeric micelle MRI contrast agent possessed the characteristic of changeable T_1-relaxivity; The polymeric micelle exhibited a lower T_1-relaxivity than did block copolymer chains having dissociated from the micelle. This changeable character can be utilized as a tumor-specific MRI contrast

* Corresponding author. Tel.: +81 44 819 2093; fax: +81 44 819 2095.
E-mail address: yp-yokoyama2093ryo@ezweb.ne.jp (M. Yokoyama).

0168-3659/$ – see front matter © 2009 Elsevier B.V. All rights reserved.
doi:10.1016/j.jconrel.2009.01.010

with a high MRI contrast (in dissociate form) at tumor tissues and a low MRI contrast (in micelle form) in the bloodstream. In the previous report, we proved this changeable character in vitro, but did not examine in vivo tumor targeting.

Several works on polymeric micelles as MRI contrast agents were reported recently [19–22]. The combination of drug targeting and imaging probes, such as MRI contrast agents, relative to polymer micelles systems has strengthened the effectiveness of chemotherapy [23]. Poly(L-glutamic acid)-*b*-polylactide and polysuccinicinimide derivatives were synthesized as a polymeric micelle-based MRI contrast agent [20,21]. Several studies have examined polymeric micelle-based MRI contrast agents, but so far, significant enhancements of MR images at solid tumors through accumulation of the polymeric micelles have not been obtained. One of the challenges that confront the use of MRI contrast agents to detect solid tumors is the selective delivery of the contrast agents to solid tumors by means of the EPR effect. From our experience of anti-cancer drug targeting with polymeric micelle carriers, we assume that an important key for successful tumor targeting is suppression of the incorporated drug's interactions with cells and proteins, in particular, hydrophobic interactions. In our previous report, we showed that polymeric micelles exhibiting lower levels of hydrophobic interactions provided higher levels of antitumor activities, possibly through more efficient passive targeting [24]. If this assumption is applied to MRI contrast agents, the micelle outer shell with a biologically inert character is preferable. Therefore, we have chosen a micelle design with the inert poly(ethylene glycol) outer shell and the contrast species (Gd ion)-containing inner core. Furthermore, we have chosen a negatively charged inner core, not a positively charged one, since positive charges are known to induce strong interactions with the reticuloendothelial system (RES) [25]. Consequently, strong interactions with the RES drastically lower the targeting efficiency relative to solid tumors.

In this report, we synthesized negatively charged block copolymers based on a poly(ethylene glycol)-*b*-poly(L-lysine) system to obtain a long-circulating polymeric micelle MRI contrast agent. This negatively charged block copolymer was found to form a polymeric micelle structure without an addition of positively charged macromolecules. Blood circulation, biodistribution, and excretion of the contrast agents were evaluated. MR images of mice were taken after an injection of the contrast agent, and these images were compared before the injection. According to the findings, polymeric-micelle MRI contrast agent appears to be a strong tool for polymeric-micelle-based drug targeting and for visualizing the location of the carriers at the solid tumor tissues.

2. Materials and methods

2.1. Materials

For the current study, α-methoxy-ω-aminopropyl-poly(ethylene glycol) (PEG-NH_2, M_w = 5200) was purchased from NOF Corporation, Tokyo, Japan, and benzene-based lyophilization was carried out before use. A chelating agent active ester, 1,4,7,10-tetraazacyclododecane-1,4,7,10-tetraacetic acid mono (*N*-hydroxysuccinimide ester) (DOTA-OSu), was purchased from Macrocyclics, Texas, USA. Deuterium solvents were purchased from Sigma-Aldrich, Tokyo, Japan. Dehydrated DMF and gadolinium chloride hexahydrate ($GdCl_3 \cdot 6H_2O$) were purchased from Wako Pure Chemicals Industries, Ltd., Tokyo, Japan. We used all these commercial reagents as purchased. The dialysis membrane Spectrapor 6 (molecular weight cut off (MWCO) = 1000) was purchased from Spectrum Laboratories Inc., Tokyo, Japan. ^1H NMR spectra were recorded on a Varian UNITY INOVA 400 MHz NMR spectrometer. To measure gadolinium ion contents in the block copolymer, we used inductively coupled plasma (ICP) with an SPS7800 apparatus (SII Nanotechnology Inc., Tokyo, Japan). Dynamic

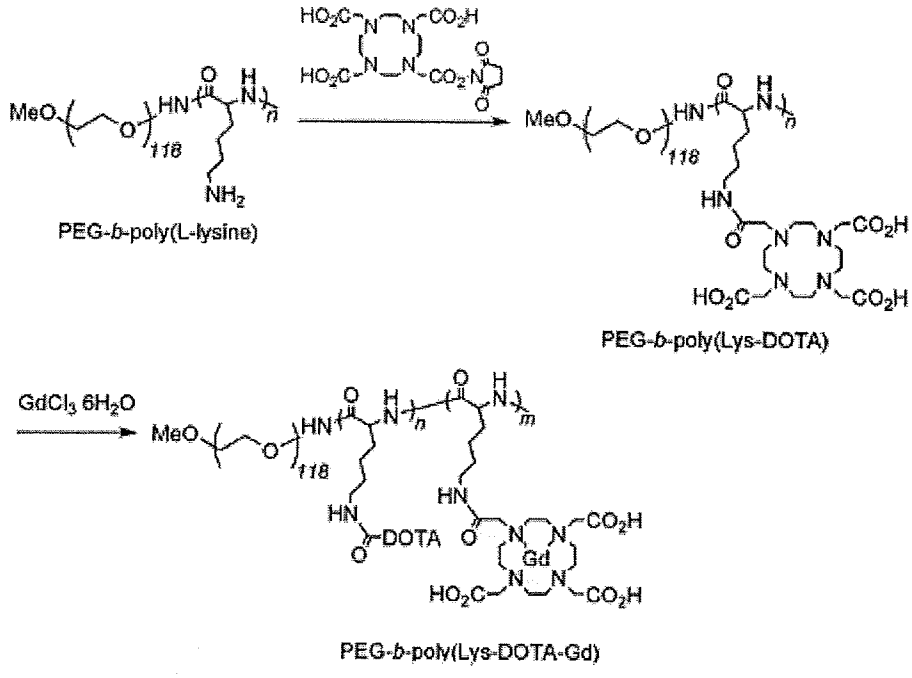

Fig. 1. Synthesis of PEG-P(Lys-DOTA-Gd).

light scattering (DLS) measurements were carried out at 24.5 °C with a DLS-700 instrument (Otsuka Electronics Co., Ltd., Tokyo Japan). Measurement of zeta-potential was performed with an ELSZ-2 instrument (Otsuka Electronics Co., Ltd., Tokyo Japan).

2.2. Animals

Five-week-old ddY female mice and CDF_1 female mice were purchased from the Sankyo Labo Service Corporation, Tokyo, Japan. All animal experiments were carried out in accordance with the guidelines of the Guiding Principles for the Care and Use of laboratory Animals of Hoshi University.

2.3. Synthesis of PEG-P(Lys-DOTA)

A synthesis of a chelate moiety-binding block copolymer is shown in Fig. 1. A poly(ethylene glycol)-*b*-poly(L-lysine) block copolymer (PEG-P(Lys)) was prepared through acid hydrolysis of a poly(ethylene glycol)-*b*-poly[ε-(benzyloxycarbonyl)-L-lysine] (PEG-P(Lys(Z)) block copolymer [26]. We synthesized PEG-P(Lys)s from PEG-NH_2 (molecular weight of PEG-NH_2 = 5200). The compositions of PEG-P(Lys)s were determined by means of ^1H NMR in D_2O under an acidic condition. A mixture of PEG-P(Lys) (86.0 mg), and 1,4,7,10-tetraazacyclododecane-1,4,7,10-tetraacetic acid mono (*N*-hydroxysuccinimide ester) (DOTA-OSu, 308.0 mg) in 8.6 mL of dry DMF was stirred, and then, dry triethylamine (0.5 mL) was added to this reaction mixture. The reaction mixture was stirred overnight at 50 °C. The resulting mixture was dialyzed, at first, against 0.02 N HCl and, then, against distilled H_2O 5 times. The obtained polymer was dissolved in H_2O (at a polymer concentration higher than 15 mg/mL) again, and dialyzed against H_2O 3 times, and we obtained poly(ethylene glycol)-*b*-poly(L-lysine-DOTA) (PEG-P(Lys-DOTA)) by means of lyophilization (162.8 mg). The composition of PEG-P(Lys-DOTA) was determined by means of ^1H NMR in D_2O under an alkali condition (pH> 10). The number of bound DOTA units per polymer chain was calculated from the peak area ratio among CH_2 protons of PEG at 3.73 ppm, 24H protons of DOTA, and 2H protons of lysine in the range of 3.36–2.18 ppm. ^1H NMR (ppm, D_2O + NaOD): 4.08 (s, CH of lysine units), 3.73 (s, CH_2 of PEG), 3.39 (s, OCH_3 of terminal PEG), 3.36–2.18 (m, 24H of DOTA and CH_2 of lysine), and 2.18–1.10 (m, 6H of lysine).

2.4. Gadolinium (III) chelation to PEG-P(Lys-DOTA)

$GdCl_3 \cdot 6H_2O$ (35.0 mg, 0.094 mmol) was added to PEG-P(Lys-DOTA) (153.3 mg) in H_2O (15.0 mL), and the pH of the solution was maintained between 6.0–6.5. The reaction mixture was stirred for 3 h at 50 °C, followed by dialysis against distilled H_2O 5 times. PEG-P(Lys-DOTA-Gd) was obtained as a white solid after lyophilization (160.8 mg). The determination of gadolinium ions in the block copolymer was carried out by means of ICP measurements (7.0 wt.%, the number of gadolinium ions per polymer chain was 6.7). The obtained PEG-P(Lys-DOTA-Gd) is indicated as 118–17–17–7 (PEG unit = 118, lysine units = 17, DOTA moieties = 17, number of gadolinium ion = 7).

2.5. Blood concentration of PEG-P(Lys-DOTA-Gd) micelles in mice

Blood samples (10–75 μL) from the tail vein (n = 3) of mice (ddY) (30–33 g) were collected in heparinized capillary glass. Saline (1.5 mL) was added to the blood samples, and the mixture was centrifuged at 4 °C for 4 min at 13,000 rpm. The supernatant of the plasma solution was collected, and the gadolinium ion contents of the block copolymer were measured by means of ICP. The plasma and blood volume were calculated as 0.0488 mL/g body weight for plasma and 0.0778 mL/g body weight for blood, respectively.

2.6. Biodistribution of the contrast agents

Biodistribution of the contrast agents was evaluated in CDF_1 female mice (5 weeks old) (20–22 g) bearing a colon 26 tumor. Colon 26 cells (1.0×10^4 cells/0.1 mL) were transplanted into CDF_1 female mice subcutaneously. Injection of the contrast agents was started 9–10 days after the transplantation. Tumor volumes were approximately 50–100 mm^3. The tumor volumes were calculated as follows: volume = $1/2LW^2$; L is the long diameter and W is the short diameter of a tumor.

Twenty-four hours after the injection, the blood was collected with a heparinized syringe and centrifuged at 4 °C for 4 min at 13,000 rpm. The plasma was obtained, and its gadolinium content was measured by means of ICP. The major tissues including tumor tissues were excised and weighted. For the determination of gadolinium ion content in the tissue, saline was added to the tissues, followed by an addition of nitric acid (conc. 70%) and sulfuric acid (conc. 98%). Then, the mixture was heated. A saturated aqueous oxoammonium solution was added to the yellow mixture and heated again. The resulting pale-yellow mixture was diluted with saline. The supernatant was collected, and its gadolinium content was measured by means of ICP. The urine (n = 3) was collected 24 h and 48 h after injection, and its gadolinium content was measured by means of ICP.

2.7. MR imaging of mice tumor model

MR imaging was performed with female mice (CDF_1) bearing a colon 26 tumor. The tumor transplantation was carried out as described in 2.6. The contrast agents were injected at a dose of 0.05 mmol of Gd/kg into a mice-tail vein. MR images were taken with a Varian NMR system at 9.4 T. T_2-weighted fast spin echo (TR = 2500 ms, ETL = 8, ESP = 4, effective TE = 48) was performed for all experiments before following the T_1-weighted gradient echo protocol. T_1-weighted gradient echo protocol was followed before the injection, immediately after the injection, and then 4 h and 24 h after the injection. Imaging parameters of the T_1-weighted images were TR/TE = 8.0/4.2, flip angle = 30°, field of view of 50 × 30 mm, a matrix size of 192 × 192, and 2 mm of coronal slice thickness, and were TR/TE = 8.0/4.5, flip angle = 30°, field of view of 45 × 45 mm, a matrix size of 192 × 192, and 2 mm of axial slice thickness. For normalized signal intensity relative to the T_1-weighted images, the tumor area was selected as a region of interest (ROI). The signal intensity of the ROI was compared with the intensity of a stock solution of 0.1 mM gadolinium ion in agarose gel. The relative signal intensity of the ROI

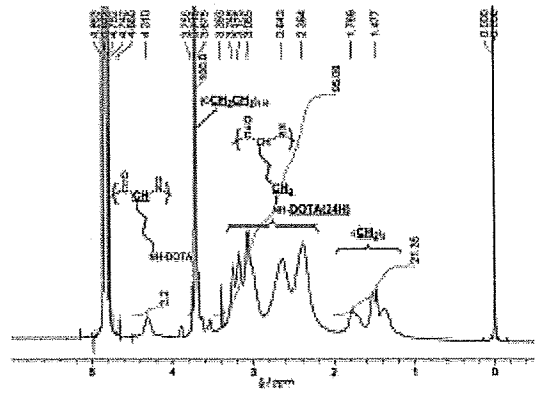

Fig. 2. ^1H NMR spectrum of PEG-P(Lys-DOTA) (118–17–17) in D_2O + NaOD.

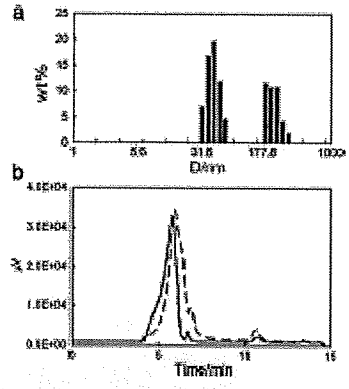

Fig. 3. (a) Weight-weight average size distribution of PEG-P(Lys-DOTA-Gd) micelle (118-17-17-7) in 150 mM NaCl measured by DLS, and (b) gel-permeation chromatogram of PEG-P(Lys-DOTA-Gd) micelle in H_2O (1.2 mg/mL) of concentrated preparation of 118-17-17-7 (solid line) and diluted preparation of 118-17-17-6 (dashed line).

24 h after the injection was compared with the signal intensity before the injection.

3. Results and discussion

3.1. Block copolymer synthesis and characterization of polymeric micelle

A block copolymer binding DOTA groups was synthesized from poly(ethylene glycol)-*b*-poly(L-lysine). The binding of a DOTA at the lysine residues was carried out with a coupling reaction between a primary amine and an NHS ester of a DOTA reagent, as shown in Fig. 1. Poly(ethylene glycol)-*b*-poly(L-lysine-DOTA) block copolymers possessing 5200 of molecular weights, and 17–21 units of the DOTA-bound lysine moiety were obtained. Quantitative substitution of lysine residues for DOTA was confirmed in ^{1}H NMR spectra as shown in Fig. 2.

A fully DOTA-substituted block copolymer formed polymeric micelles after the dialysis in dist. H_2O at a polymer concentration of 15 mg/mL. The quantitative DOTA conjugation was essential for the polymeric micelle formation. Insufficient DOTA conjugation, such as 118-22-19 wherein the number of DOTA residues was 19 out of 22 lysine residues, did not form a polymeric micelle. This result shows that the micelle structures were not formed in the presence of a small amount of unmodified lysine residue (3 out of 22 residues); the result also underscores the importance of strong interactions among the conjugation DOTA units for the micelle formation.

Gadolinium ion was partially chelated to DOTA in the block copolymer, poly(ethylene glycol)-*b*-poly(L-lysine-DOTA). Gadolinium-chelated poly(ethylene glycol)-*b*-poly(L-lysine-DOTA-Gd) maintained the polymeric micelle formation. Dynamic light scattering (DLS) and GPC measurements of the gadolinium chelated block copolymers, 118-17-17-7 which is 118 ethylene glycol units, 17 lysine residues, 17 DOTA conjugation to lysine residues, and 7 gadolinium ions at DOTA were performed. Fig. 3(a) shows a DLS chart of this block copolymer micelle with a weight average of 42.9 ± 7.6 nm (mean ± SD), accompanied by a secondary aggregation of a weight average of 225.5 ± 53.0 nm (mean ± SD). Similar secondary aggregation was also found in the precursor of PEG-*b*-poly(L-lysine-DOTA-Gd) (data in supplemental section).

The zeta-potential of the obtained polymeric micelle showed −9.55 mV in 150 mM NaCl solution, indicating that the polymeric micelle was negatively charged. This negative value was given from a vacant DOTA moiety having 3 carboxylic acids and 4 tertiary amines. The tertiary amines of DOTA could work as only two cationic species in the physiological condition owing to their excessively close proximity to each other, whereas three carboxylic acids in the DOTA moiety could work as 3 anions owing to their long distances from one other. As a result, the total charge of the polymeric micelles exhibited negatively charged particles. In general, cationic species are more quickly scavenged by the reticloendothelial system than anionic species [25]. This scavenging is a big obstacle for the passive tumor targeting through the EPR effect. For the design of a tumor-targeting system, a slightly negative-charged particle is preferable as an inert carrier.

GPC measurements of the polymeric micelle (1.2 mg/mL in H_2O) were performed by the use of an HPLC system (LC 2000 series, Jasco, Tokyo, Japan) equipped with a TSK-gel G4000-PW$_{XL}$ column (eluent = H_2O, flow rate = 1.0 mg/mL, detector = RI) at 40 °C. Even in such a diluted aqueous solution of the block copolymer, both DLS and GPC measurements clearly exhibit the formation of the polymeric micelle as shown in Fig. 3(b) (solid line). This finding indicated that once the polymeric micelle was formed by interactions among vacant DOTAs, the polymeric micelle was not dissociated in a time scale of a DLS and GPC measurement under dilution. When we injected a similar sample 118-17-17-6 prepared from a dilute condition (3 mg/mL), the peak of the polymeric micelle was shifted to a longer elution time as shown in Fig. 3(b) (dashed line). This result indicates a considerable polymer concentration effect on the formation of the polymeric micelle; namely, strong interactions among vacant DOTA moieties at a high concentration.

Formation of the polymeric micelle with or without a gadolinium ion appears to depend on interactions among vacant DOTAs as described above. To prove this interaction, we added an excess of $GdCl_3$ (2.0 mol equivalent vs DOTA) into 118-20-20 to prepare complete chelation of the DOTA units with gadolinium ions. However, we found that the composition of the block copolymer was 118-20-20-16. Even when we added the excess amount of gadolinium ions to the block copolymer, we obtained 20% of vacant DOTA in the block copolymer. This result implies that DOTA–DOTA interactions prevent gadolinium ion from freely chelating into a DOTA moiety. When we injected this block copolymer into the GPC column, we observed that the peak of around 5–6 min. corresponded to the polymeric micelle disappeared. This disappearance indicates that chelation of a high level of gadolinium ion in a block copolymer resulted in so unstable micelle formation on the GPC column. We concluded that the polymeric micelle was formed through the interactions among vacant DOTAs, and that these interactions depend on the block copolymer concentrations and on the numbers of the chelated gadolinium ions.

3.2. Blood circulation of the polymeric micelle MRI contrast agent

The polymeric micelle, 118-17-17-7, was injected at a dose of 0.05 mmol Gd/kg, into a mouse-tail vein for pharmacokinetic

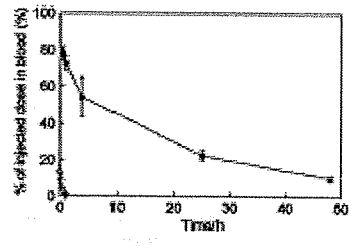

Fig. 4. Blood-concentration time course of PEG-P(Lys-DOTA-Gd) micelle (118-17-17-7) in ddY female mice at a dose of 0.05 mmol Gd/kg (■), and Gd-DTPA at a dose of 0.10 mmol Gd/kg (◇). After defined time periods (0.5 h, 1 h, 2 h, 4 h, 24 h, and 48 h), the blood samples were collected into capillary glass tubes via mice's tail veins.